

1 An improved modelling chain for bias-adjusted high-resolution 2 climate and hydrological projections for Norway

3 Shaochun Huang¹, Wai Kwok Wong¹, Andreas Dobler³, Sigrid Jørgensen Bakke¹, Stein Beldring¹,
4 Ingjerd Haddeland^{1*}, Hans Olav Hygen³, Tyge Løvset², Stephanie Mayer², Kjetil Melvold¹, Irene Brox
5 Nilsen¹, Gusong Ruan¹, Silje Lund Sørland^{2^}, Anita Verpe Dyrørdal³

6 ¹Department of Hydrology, Norwegian Water Resources and Energy Directorate, Oslo, 0301, Norway

7 ²NORCE Research AS, and Bjerknes Centre for Climate Research, Bergen, 5008, Norway

8 ³Department of Climate and Environment, Norwegian Meteorological Institute, Oslo, 0371, Norway

9 [^]now at SWECO AS, Bergen, Norway

10 ^{*}now at Lyse AS, Stavanger, 4018, Norway

11 *Correspondence to:* Shaochun Huang (shh@nve.no)

12 **Abstract**

13 About every 10 years, the Norwegian Centre for Climate Services publishes a national climate assessment report, presenting
14 the updated historical climate change and climate projections towards the end of this century. This paper documents the model
15 experiment used to generate high-resolution climate and hydrological projections for the new climate assessment report
16 published in October 2025. The model experiment follows the standard modelling chain for hydrological impact assessment,
17 i.e., climate model selection - downscaling and bias adjustment - hydrological modelling. However, compared with the model
18 experiment for the climate assessment report published in 2015, all modelling components have been improved in terms of
19 data availability, data quality and methodology. Specifically, a large climate model ensemble was available and new criteria
20 were developed to select tailored climate projections for Norway. Two bias-adjustment methods (one univariate and one
21 multivariate) were applied to account for the uncertainty of method choice. The hydrological modelling was improved by
22 implementing a physically-based Penman-Monteith method for evaporation and a glacier model accounting for glacier retreat
23 under climate change scenarios. Besides model description, this paper elaborates the effects of different bias-adjustment
24 methods and the contribution of climate models and bias-adjustment methods to the uncertainty of climate and hydrological
25 projections under the RCP4.5 scenario as examples. The results show that the two bias-adjustment methods can contribute
26 larger uncertainty to seasonal projections than climate models. The multivariate bias-adjustment method improves hydrological
27 simulations, especially in the reference period, but cannot conserve climate change signals of the original climate projections.
28 The dataset generated by the presented modelling chain provides the most updated, comprehensive and detailed
29 hydrometeorological projections for mainland Norway, serving as a knowledge base for climate change adaptation to decision
30 makers at various administrative levels in Norway.

33 **1 Introduction**

34 It is unequivocal that human influence has warmed the climate at a rate that is unprecedented in at least the last 2000 years
35 (IPCC, 2021). The human-induced warming has already modified the global hydrological cycle, leading to significant shifts
36 in the spatial and temporal patterns of hydrological components (Gu and Adler, 2015; Gudmundsson et al., 2021; Li et al.,
37 2023) and more intensive and frequent hydroclimatic extreme events (Alifu et al., 2022; Chinita et al. 2021; Dunn et al., 2020;
38 Padrón et al., 2020). These impacts pose unprecedented challenges for water resource management at regional and local scales,
39 and they are expected to be more severe in the future if unsustainable development continues (Wang and Liu, 2023). Therefore,
40 understanding of the potential climate change impact from a long-term and systematic perspective serves as a key basis to
41 develop climate adaptation strategies, such as incorporating climate projections into European building standards (EEA, 2025)
42 and national climate risk adaptations (DCCEW, 2023).

43 General circulation models (GCMs) are important tools to understand and predict climate behavior under various greenhouse
44 gas emission scenarios on the global scale. GCMs have been developed rapidly in the last decades, with an increasing number
45 of models from over 40 within the Coupled Model Intercomparison Project phase 5 (CMIP5, Taylor et al., 2012) for
46 Representative Concentration Pathway (RCP) emission scenarios to over 60 within CMIP6 (Eyring et al., 2016) for the Shared
47 Socioeconomic Pathways (SSP) emission scenarios. Such a large ensemble of models provides valuable information of
48 uncertainty for future climate projections, accounting for natural climate variability, unknown socio-economic developments,
49 and model differences (Hawkins and Sutton, 2011). However, the use of the full ensemble can be challenging for impact
50 models due to computational restrictions, so it often requires a careful selection of projections for specific study areas based
51 on comprehensive analysis of the whole ensemble (Dalelane et al., 2018). In addition, GCM outputs are hardly applied for
52 impact assessment at regional and local scales due to their coarse spatial resolutions (e.g., ~ 0.25 to 3° for the CMIP6 models
53 and ~ 0.5 to 4° for the CMIP5 models) and systematic biases (Rössler et al., 2019), and they are usually downscaled to fine
54 spatial resolutions and bias adjusted for climate impact assessment and adaptation planning (Martinich and Crimmins, 2019).

55 The GCM outputs can be downscaled dynamically using regional climate models (RCMs) or statistically based on statistical
56 relationships between coarse-resolution variables in GCMs and fine-resolution or local observations in the historical period
57 (Zhang et al., 2020). Various RCMs and statistical downscaling methods have been developed and applied to downscale the
58 GCM outputs, increasing the number of climate projections for region scales. For example, the European Coordinated Regional
59 Downscaling Experiment (EURO-CORDEX, Jacob et al., 2020) applies 11 RCMs to downscale the outputs from 14 GCMs to
60 0.11° (ca. 12.5 km) horizontal resolution. Due to the high computational cost and time consumption, each RCM is able to
61 downscale one or a few GCMs outputs, resulting in 30, 25 and 64 regional climate projections for Europe under the RCP2.6,
62 RCP4.5 and RCP8.5 scenarios, respectively. In contrast, statistical downscaling methods, which are often combined with bias

63 adjustment, can be easily applied for a large ensemble of GCMs due to low computational requirements and fast calculations,
64 and over 50 statistical downscaling methods have been applied for Europe (Gutiérrez et al., 2019).

65 Each downscaling method has its strengths and weaknesses. The dynamic downscaling ensures the physical relationships
66 between climatic variables and spatial dependence, but it inherits significant biases from GCMs and requires further bias
67 adjustment and/or statistical downscaling depending on the scale of impact studies (Hundecha et al., 2016; Maraun og
68 Widmann, 2018). In contrast, the statistical downscaling usually outperforms the RCMs in terms of bias, but many methods
69 downscale individual climatic variables independently. As univariate bias-adjustment methods, this approach does not modify
70 inter-variable dependency structures but keeps them as in the original model data which can be inaccurate. Eum et al. (2020)
71 demonstrated different impact of univariate and multivariate statistical downscaling methods on reproduction of snowfall and
72 recommended the use of the multivariate methods for climate change impact assessment in snow-dominated watersheds. Meyer
73 et al. (2019) also found underestimation of snow accumulation (up to 50%) in alpine catchments when using univariate contra
74 multivariate bias-adjustment approach, which can be attributed to less precipitation below temperatures of 0 °C.

75 Due to the large number of GCM projections and downscaling methods, as well as their strengths and weaknesses, to construct
76 a downscaled and bias-corrected ensemble for specific regions is challenging. Different choices of GCM and downscaling
77 methods can lead to considerably different local climate projections and thus contribute large uncertainty to local decision-
78 relevant climate outcomes (Tang et al., 2016; Lafferty and Sriver, 2023). In addition, they result in different climate impact
79 projections for streamflow (Kay, 2025), flood hazard (Kundzewicz et al., 2017), agriculture (Li et al., 2023), ecosystem
80 (Pourmokhtarian et al., 2016), etc, causing inconsistent impact assessments not only within each impact sector but also across
81 sectors. Therefore, a consistent and tailored ensemble of regional climate projections is highly appreciated for each region and
82 many countries have put great efforts to create national ensembles of climate projections (Golding et al., 2025), such as
83 Switzerland (Fischer et al., 2022), Germany (Hübener et al., 2017), UK (Reyniers et al., 2025) and Australia (Peter et al.,
84 2024).

85 Norway is located in the northern high latitudes, which have experienced the strongest warming since 1980 among all regions
86 in the world, with warming trends spanning from 0.2 to more than 0.6 °C/decade (IPCC, 2021). The strong warming in the
87 historical period raises great attention from both the scientific community and the public to future climate change and its
88 impacts on hydropower production (about 90% of total power production in the country), winter tourism (skiing), and water
89 related natural hazards (i.e., flood, drought, avalanche and landslide). However, it is specifically challenging to construct robust
90 and reliable climate projections as well as hydrological impact projections in Norway, due to the high heterogeneity in
91 topographic and hydroclimatological characteristics.

92 Norway is one of the most mountainous countries in Europe, with more than 90% of the landscape consisting of mountains.
93 The rugged topography leads to a complex spatial and temporal pattern of temperature and precipitation, varying with

94 geographical position, elevation, aspect (slope direction), and slope angle (Dobrowski et al., 2009; Franke, 2024). The spatial
95 resolutions of the state-of-the-art GCMs and RCMs are too coarse to provide sufficient spatial variations of climate for such
96 complex terrain. In addition, these projections often show a cold bias for Norway (Wong et al., 2016), which for example leads
97 to a prolonged snow season, low winter runoff and late snowmelt in hydrological projections (Nilsen et al., 2021).

98 In order to construct a consistent and tailored ensemble of national climate projections as well as hydrological projections for
99 Norway, the Norwegian Centre for Climate Services (NCCS) brings together experts from the Norwegian Meteorological
100 Institute, the Norwegian Water Resources and Energy Directorate (NVE), the Norwegian Research Centre (NORCE) and
101 Bjerknes Centre for Climate Research. NCCS is responsible for the national climate assessment report, updated about every
102 10 years, which presents updated historical climate change and climate projections towards the end of this century and serves
103 as a knowledge base for climate change adaptation to decision makers and planners at various administrative levels in Norway
104 (Nilsen et al., 2022). The previous climate assessment report “Climate in Norway 2100” (Hanssen-Bauer et al., 2015; hereafter
105 abbreviated CiN-2015), published in 2015, was based on 10 available GCM-RCM combinations within the CMIP5 and EURO-
106 CORDEX frameworks. The projections were further re-gridded and bias-adjusted into 1×1 km resolution using empirical
107 quantile mapping and forced the distributed version of the HBV (Hydrologiska Byråns Vattenbalansavdelningen, i.e. “The
108 Hydrological Bureau’s Water Balance Department”) hydrological model (distHBV, Beldring et al., 2003) to generate
109 hydrological projections. This spatial resolution is the result of the need to serve projections that can be used locally on the
110 one hand, and availability of computational resources and reference datasets to produce daily maps for the whole of Norway
111 on the other. During the last 10 years, all methods along the modelling chain, including GCMs, RCMs, climate model
112 selections, statistical downscaling and bias correction, and hydrological models, have been further developed, and the
113 observation data has been updated and improved. These developments promote the new generation of high-resolution and
114 bias-adjusted climate and hydrological projections, which are more robust than the previous ones in CiN-2015.

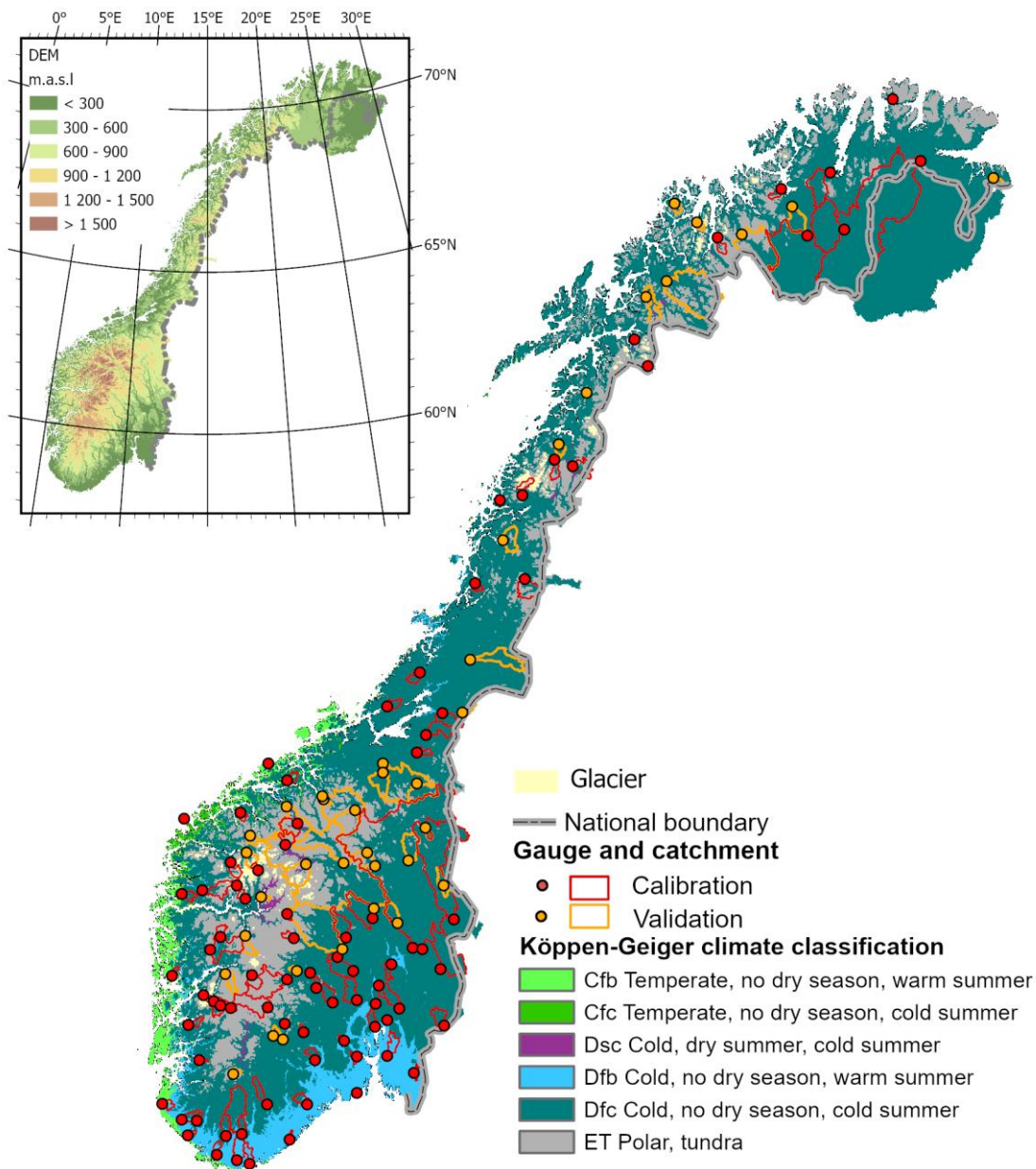
115 In this paper, we present the full description of the methods to produce the updated downscaled and bias-adjusted climate
116 projections and hydrological projections for the new climate assessment report for Norway “CiN-2025” (Dyrrdal et al., 2025),
117 specifically focusing on selection of GCM-RCMs combinations, statistical downscaling and bias-adjustment and hydrological
118 modelling. Section 2 introduces the study area and historical input data. The methods described include the overview of the
119 whole modelling chain (Section 3), selection of atmospheric variables from a set of EURO-CORDEX simulations (Section 4),
120 statistical downscaling and bias-adjustment method (Section 5) and hydrological modelling (Section 6). In Section 7 and 8,
121 we present the climate and hydrological products and uncertainty analysis. Finally, we discuss the limitations of the methods
122 and the potential applications of the products, and point out the way towards the next generation of national climate projections
123 for Norway in Section 9.

124 **2 Study area and historical data**

125 **2.1 Study area**

126 The modelling domain of this study is the mainland of Norway and a few river catchments draining from neighbouring
127 countries (Sweden and Finland) (Fig. 1), resulting in 354448 1x1 km² grid cells. Due to large variations in latitude and altitude,
128 Norway exhibits six climate regimes according to the Köppen-Geiger climate classification (Beck et al., 2018), ranging from
129 temperate climate along the west coast to polar climate in high mountains and in the north (Fig. 1). The average elevation of
130 Norway is about 460 m, ranging from 0 along the coast to 2469 m at Galdhøpiggen in the center of the country. Open firm
131 ground and forest are the two major land covers in Norway, accounting for 36% and 37.8% of the mainland area, respectively
132 (Statistics Norway, 2025). There are also large areas of bedrock (8.5%), followed by water (6.2%), bogs (5.4%), agricultural
133 land (3.5%) and built-up (1.7%). About 1% of mainland Norway is covered by glaciers (Fig. 1). The mean annual temperature
134 in the current standard normal period 1991–2020 ranges from -9.5 to +9.5 °C (Tveito, 2021). The warmest areas are found in
135 lower-lying areas in southern Norway, and particularly along the coast in the southwest, while the coldest areas are in the high
136 mountains and inland areas of the north. Norway also exhibits large spatial variability in precipitation, ranging from 212 mm
137 in southern parts of Northern Norway to 6130 mm close to the Ålfotbreen glacier in Western Norway. The wet areas along the
138 west coast are exposed to migrating low pressure systems most often arriving from the west-southwest (Lutz et al., 2024).

139 We selected 85 and 38 catchments for calibration and validation of the hydrological model, respectively. All these catchments
140 are near-natural catchments and 112 of the 123 catchments are smaller than 1000 km². The distribution of the catchments
141 represents various climate and hydrological regimes, geographic conditions and landscape types in Norway. The catchment
142 boundary is delineated by NVE and the gauges at the outlet of these catchments are shown in Fig. 1.



143

144 **Figure 1: the climatic and topographic characteristics of the simulation domain as well as the locations of glaciers and hydrological**
 145 **gauging stations and catchment boundaries.**

146 **2.2 Historical meteorological data**

147 The historical meteorological data is used as reference in the bias-adjustment procedures and for hydrological model calibration
148 and validations. It consists of nine atmospheric meteorological variables at a 1 x 1 km² grid covering Norway and river
149 catchments in neighbouring countries (Fig. 1): mean, minimum and maximum 2m temperature (K), precipitation flux (mm/s),
150 relative humidity (%), longwave and shortwave radiation (W/m²), pressure (Pa) and 10m wind speed (m/s).

151 Daily minimum, maximum and mean temperatures as well as precipitation are provided by the seNorge2018 v20.05 dataset
152 (Lussana et al., 2019; 2020). It covers the period 1957–2020 and is based on quality-assured daily datasets. The precipitation
153 values are adjusted for wind-induced under-catch based on Wolff et al. (2015). Note that seNorge2018 continuously
154 incorporates the latest available station data and is therefore not homogenized in time. This may affect the calculation of
155 changes within the historical period.

156 Daily wind speeds for Norway from 1958 to 2020 are obtained from the KliNoGrid 16.12 dataset. The KliNoGrid dataset is
157 based on the Norwegian atmospheric reanalysis NORA10 (Reistad et al., 2011) wind speed data, downscaled onto a 1 km grid
158 using a quantile mapping approach (Bremnes, 2004) to match the climatology of the high-resolution numerical weather
159 prediction model AROME-MEtCoOp (Müller et al., 2017).

160 Daily short- and longwave radiation, relative humidity and surface pressure are obtained from the HySN2018v2005ERA5
161 dataset. It is generated based on the ECMWF atmospheric reanalysis ERA5 (Hersbach et al., 2020) and seNorge2018 v20.05
162 and covers the period 1958–2020. The dataset is described in detail in Huang et al. (2022) and Erlandsen et al. (2021).

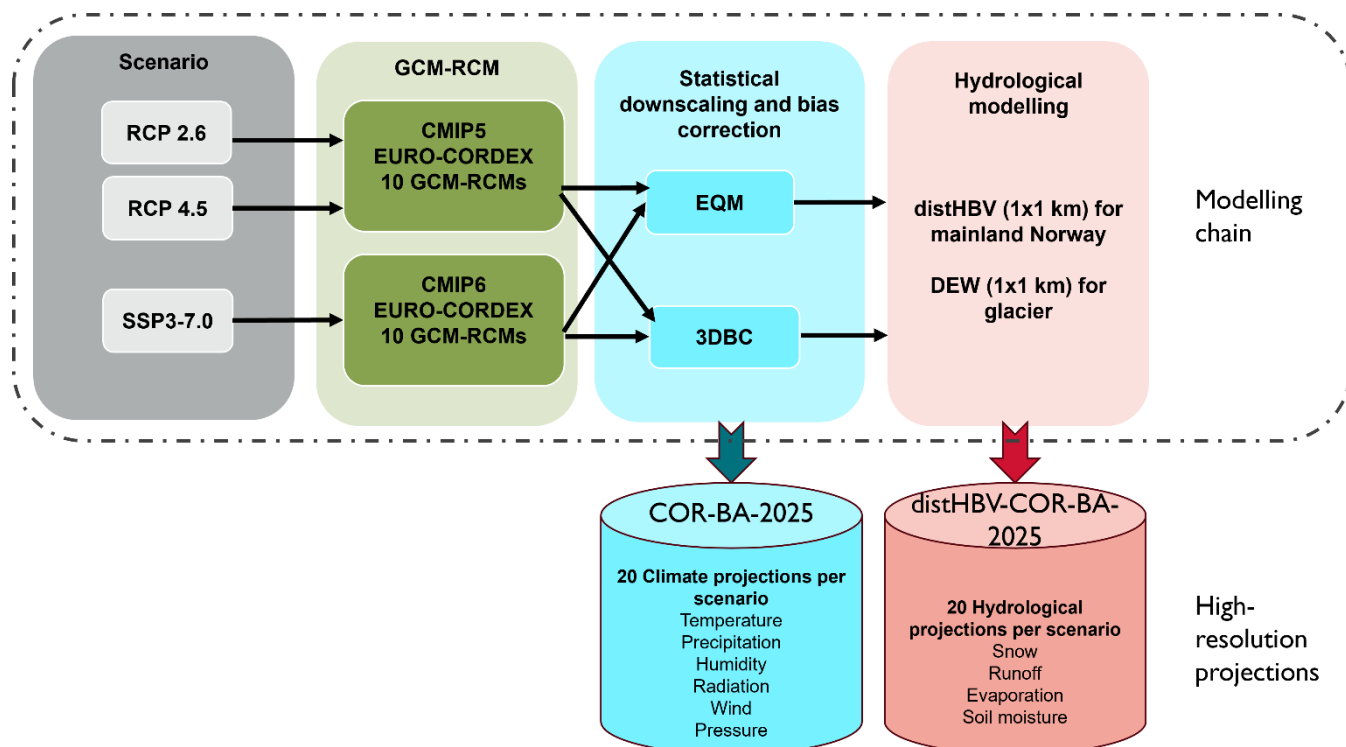
163 **2.3 Data for setting-up hydrological models**

164 To set up the hydrological model, a digital elevation model (DEM), as well as maps of soil type and land cover type with 1
165 km horizontal resolution are required. The DEM map was provided by the Norwegian Mapping Authority. Five soil types are
166 reclassified based on the sediment map from the Geological Survey of Norway (Erlandsen et al., 2021), and bare mountain
167 soil and moraine soils account for ca. 80% of the total mainland area. Nine land cover types (open area, bog, built-up, forest,
168 cropland, heather, bedrock, lake, permanent ice and snow) are classified based on the National Land Resource Map (Ahlstrøm
169 et al., 2014) and the remote sensing based forest resource map SAT-SKOG (Gjertsen and Nilsen, 2012). The forest land cover
170 is further classified into 12 structural forest types to distinguish three species groups (spruce, pine, and deciduous forest) and
171 four forest development stages (underdevelopment, two intermediate development stages and mature forest) (Majasalmi et al.,
172 2018). The parametrization for each forest structural type, such as maximum leaf area index, vegetation height and shortwave
173 albedo, is given by Majasalmi et al. (2018) and Bright et al. (2018). For glacier areas, the glacier modelling doesn't account
174 for variation of soil types and uses simplified land cover types including open area, bog, forest, bedrock and glacier area
175 coverage. However, it requires glacier ice thickness and glacier area data (Andreassen et al. 2015) to setup the model.

176 Discharge measurements from 123 gauging stations are used to calibrate and validate the hydrological model (Fig. 1). They
177 are quality-assured by NVE. All 123 stations have measured daily discharge from 1980 to 2014 with less than 5% missing
178 data. For the glacier modelling, mass balance data is only available for six glaciers and discharge measurements from 19
179 gauging stations downstream of the glaciers are used to calibrate and validate the hydrological model. All discharge and mass
180 balance data are publicly available at sildre.nve.no and glacier.nve.no/glacier/viewer/ci/en/.

181 **3 Modelling chain**

182 We followed the commonly used modelling chain in hydrological climate impact studies, i.e., 1) emission scenarios, 2) GCMs
183 and RCMs, 3) statistical downscaling and bias correction and 4) hydrological model (Fig. 2). The first component of the
184 modelling chain is to select emission scenarios. For the CiN-2025 report, two RCPs used in CMIP5 were selected, representing
185 a very stringent pathway (RCP2.6) and a moderate-emissions pathway (RCP4.5). The shared socioeconomic pathway SSP3-
186 7.0 used in CMIP6 was selected to represent the high-emission scenario. The reason why only one SSP scenario was selected
187 is that SSP1-2.6 and SSP3-7.0 were the first-priority scenarios for the EURO-CORDEX community (Katragkou et al., 2024).
188 The data has become available late with regard to the time needed to run our complete modelling chain - it is in fact still not
189 openly available - making the selection of more than one SSP scenario infeasible. Such a combination of CMIP5 and CMIP6
190 scenarios has also been used in other national climate projections, e.g., the climate projections in Switzerland published at the
191 end of 2025 (Schumacher et al., 2024) which combined EURO-CORDEX RCP8.5 with CMIP6 SSP5-8.5 GCM simulations.



192
193 **Figure 2: Modelling chain to generate high-resolution climate and hydrological projections for the CiN-2025 report.**

194 In the second component of the modelling chain the task is to select a representative model ensemble from the EURO-
195 CORDEX simulations (Jacob et al., 2014) for each emission scenario. Within the EURO-CORDEX framework, CMIP5 and
196 CMIP6 GCMs are downscaled by different RCMs, resulting in a set of GCM-RCM combinations. For CiN-2025 a larger
197 EURO-CORDEX ensemble for RCP scenarios was available compared to CiN-2015, enabling a more robust data basis and
198 requiring new model selection strategies (Section 4).

199 Once the model ensemble was identified, the next step was to downscale the RCM projections of atmospheric variables from
200 the original grid size of approximately 12.5 km to 1 km. It was followed by removal of biases in RCM simulations relative to
201 observed meteorological data (Section 2.2) in the calibration period. For future projections, we adjusted the values based on
202 the corrections established in the calibration period under the assumption that the relationship between the observed and
203 modelled data remains unchanged. Two bias-adjustment methods were used: de-trended empirical quantile mapping (denoted
204 as EQM hereafter for simplicity) and three-dimensional bias-correction (3DBC) additionally to EQM (Section 5). The former
205 is a widely used univariate bias-adjustment method and was used for CiN-2015. The latter adds a post-processing procedure,
206 taking into account inter-variable dependencies. To our knowledge, this is the first time the 3DBC method is applied in
207 Norway, and we have identified several strengths and weaknesses with this multivariate method (Section 5.3). Since the two
208 bias-adjustment methods complement each other, we decided to apply both bias-adjustment methods on the RCM projections

209 and provided two complete datasets (EQM only and EQM with 3DBC). To assess the uncertainty in the climate and
210 hydrological projections from the choice of methods, we have carried out an uncertainty analysis (Section 7.3 and 8.3).

211 The last component of the modelling chain is hydrological modelling. The distHBV model was still the main tool for simulating
212 hydrological components under different climate scenarios for the CiN-2025 report, but two major improvements have been
213 made since CiN-2015. The first improvement was to replace the temperature-based evaporation method with the Penman-
214 Monteith equation in the distHBV model (Huang et al., 2019), because physical-based approaches, such as the Penman-
215 Monteith method, consider more climatic variables and provide more robust changes in potential evaporation under climate
216 scenarios than the empirical ones (McAfee, 2013; Tam et al., 2024). The second improvement was the use of Distributed
217 Element Water balance model (DEW) (Beldring, 2008) for glacierized regions. Since distHBV was not able to simulate the
218 changes in glacier area, glacier melt water can be unrealistically simulated under climate scenarios. In contrast, DEW is able
219 to simulate glacier area, volume and surface elevation dynamically and thus gives more reliable hydrological projections under
220 climate change for glacierized regions. Both models ran independently at 1 km spatial resolution and with daily time steps, but
221 distHBV ran for all grid cells in Norway and DEW only ran for the grid cells covering glacierized regions. A postprocessing
222 procedure was carried out to combine the distHBV and DEW outputs to generate final runoff projections for mainland Norway.

223 The modelling chain resulted in two datasets with a spatial resolution of 1x1 km at daily time steps, which will be serving as
224 the basis for climate impact assessment in mainland Norway. The first dataset is termed COR-BA-2025 (short for CORDEX-
225 Bias Adjusted, updated in 2025), consisting of 20 bias-adjusted high-resolution climate projections for each emission scenario
226 and is available from 1970 to 2100 (2098 depending on GCMs). These projections include nine atmospheric variables at 1x1
227 km spatial resolution and with daily time steps, each bias-adjusted both with EQM and 3DBC: mean, minimum and maximum
228 2m temperature (K), precipitation flux (mm/s), relative humidity (%), longwave and shortwave radiation (W/m²), surface air
229 pressure (Pa) and 10m wind speed (m/s). The second dataset is called distHBV-COR-BA-2025 and consists of 20 hydrological
230 projections for each emission scenario at the same spatial and temporal resolution and coverage as the atmospheric projections.
231 The hydrological projections include two flux variables (runoff and evaporation) representing average values over each grid
232 cell in mm/day, and two state variables (soil moisture and snow water equivalent), which describe the average condition of the
233 hydrological components in a grid cell with unit mm. The evaporation, soil moisture and snow water equivalent projections
234 were generated by distHBV, whereas the runoff projections were obtained by superimposing the results of the glacierized grid
235 cells from the DEW model on the runoff projections from distHBV.

236 To select the climate ensembles and assess future changes in climate and hydrology, we defined one reference period (1991–
237 2020) and two future periods (2041–2070 and 2071–2100). The reference period was selected by two factors: 1) a recent
238 climate period better represents today’s climate, and 2) 1991–2020 is the current standard normal period defined by the World
239 Meteorological Organization (WMO). However, in CMIP5 and CMIP6, the historical simulation runs end in 2005 and 2014,

240 respectively. Data from the emission scenario RCP4.5 was used to extend the historical period beyond 2005 for RCPs and the
 241 data from the emission scenario SSP3-7.0 was used to extend the historical period beyond 2014 for SSPs.

242 Since the main focus of this paper is on the description of the methods in the modelling chain rather than assessing climate
 243 and hydrological projections under different emission scenarios, we mainly present the methods and results for the RCP4.5
 244 scenario as examples in the following sections. However, the methods described in this paper are valid for all three scenarios.

245 **4 Selection of GCM–RCM combinations**

246 Currently, the EURO-CORDEX CMIP5 projections comprise the largest high-resolution regional climate model ensemble for
 247 Europe and Norway with more than 30 simulations based on RCP2.6, more than 20 simulations based on RCP4.5 and more
 248 than 70 simulations based on RCP8.5. However, there are (only) 17 model combinations covering all three RCPs (Table 1).
 249 To be able to do a proper comparison between future projections of different RCPs, it is important to use identical model
 250 combinations for each RCP. These identical model combinations comprise five GCMs, namely CNRM_CM5, EC_EARTH,
 251 HadGEM2-ES, MPI-ESM-LR and NorESM1-M. Given time and computational constraints, we defined an upper limit of ten
 252 model combinations that are used as forcing data for the hydrological models, thus seven model combinations had to be
 253 excluded.

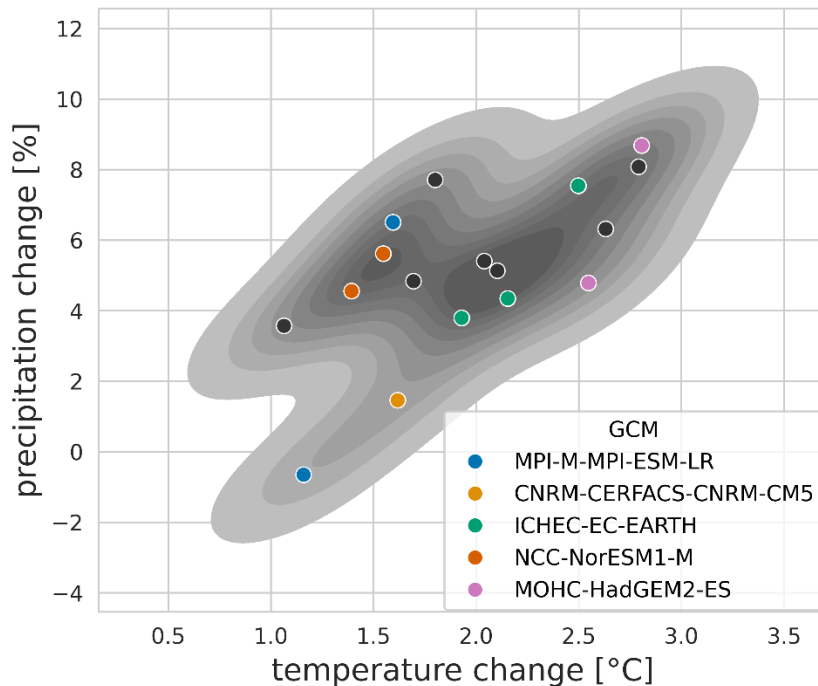
254 **Table 1. Summary of the 17 GCM-RCM combinations available for RCP2.6, RCP4.5 and RCP8.5. Combinations in bold were**
 255 **selected for downscaling and bias-adjustment for the mainland of Norway.** ¹: Original data has 360 days only. Additional days added.
 256 ²: Leap-year days added. ³: Spatial smoothing applied to tasmin, tasmax, tas and hurs.

Model combination name	GCM institute	modelling	GCM	RCM institute	modelling	RCM	Data coverage
cnrm-r1i1p1-aladin	CNRM-CERFACS		CNRM-CM5	CNRM		ALADIN63	1951–2100
ecearth-r12i1p1-rca³	ICHEC		EC-EARTH	SMHI		RCA4	1970–2100
ecearth-r12i1p1-cclm	ICHEC		EC-EARTH	BTU & KIT (CLMcom)		CCLM4-8-17	1950–2100
ecearth-r3i1p1-hirham³	ICHEC		EC-EARTH	DMI		HIRHAM5	1951–2100
hadgem-r1i1p1-rca^{1,3}	MOHC		HadGEM2-ES	SMHI		RCA4	1970–2098

hadgem-r1i1p1-remo¹	MOHC	HadGEM2-ES	GERICS	REMO2015	1950–2098
mpi-r1i1p1-cclm	MPI-M	MPI-ESM-LR	BTU (CLMcom)	CCLM4-8-17	1950–2100
mpi-r2i1p1-remo	MPI-M	MPI-ESM-LR	MPI-CSC	REMO2009	1951–2100
noresm-r1i1p1-rca^{2,3}	NCC	NorESM1-M	SMHI	RCA4	1970–2100
noresm-r1i1p1-remo	NCC	NorESM1-M	GERICS	REMO2015	1950–2100
cnrm_r1i1p1_alaro	CNRM-CERFACS	CNRM-CM5	RMIB-UGent	ALARO-0	1950–2100
cnrm_r1i1p1_racmo	CNRM-CERFACS	CNRM-CM5	KNMI	RACMO22E	1950–2100
ecearth-r12i1p1_racmo	ICHEC	EC-EARTH	KNMI	RACMO22E	1950–2100
ecearth_r12i1p1_remo	ICHEC	EC-EARTH	GERICS	REMO2015	1950–2100
hadgem_r1i1p1_racmo ¹	MOHC	HadGEM2-ES	KNMI	RACMO22E	1950–2098
hadgem_r1i1p1_hirham ¹	MOHC	HadGEM2-ES	DMI	HIRHAM5	1951–2098
mpi_r1i1p1_remo	MPI-M	MPI-ESM-LR	MPI-CSC	REMO2009	1951–2100

257

258 As a first quality check we used Table 6 in McSweeney et al. (2015) to see if the five GCMs perform satisfactorily in the
259 representation of two out of the three physical phenomena consisting of i) annual temperature and precipitation cycles, ii)
260 circulation and iii) storm tracks. This criterion did not lead to any exclusion of the 17 model combinations. As a next check
261 we verify if the GCM-RCM combinations are ranked in the ‘best half’ for 24 variables and impact-based indices (Table 2 in
262 Vautard et al., 2021) for the region of Scandinavia (Figure 12a in Vautard et al., 2021). This made us exclude cnrm
263 _r1i1p1_alaro. Further, we excluded three simulations performed with the RCM RACMO22E which are affected by a bug in
264 the snow albedo which again strongly affects the temperature signal above and around glaciers. This bug is documented in the
265 [EURO-CORDEX Errata table](#). Lastly, we checked the GCM-RCMs’ performance with respect to the observed temperature
266 and precipitation climate in Norway by using the seNorge v20.05 dataset as reference data. The largest precipitation biases (>
267 14 %) were found for the historical simulations with hadgem2_r1i1p1_hirham, mpi-r1i1p1_remo and ecearth-r12i1p1_remo,
268 hence we excluded these simulations.



269

270

271

272

273

Figure 3. Projected changes in temperature and precipitation for mainland Norway by the end of the century relative to the reference period (1991–2020) under the RCP4.5 scenario (all dots). The grey shaded area indicates the distribution (kernel density estimate) of the projected changes comprising all 17 GCM-RCM combinations that were considered. The individual coloured points highlight the ten simulations selected for CiN-2025 (Table 1).

274

275

276

277

This leaves us with ten selected model combinations presented in Table 1. The projected changes in temperature and precipitation are shown for each model combination in Fig. 3. Based on the selected ten GCM-RCM combinations (coloured dots in Fig. 3), the projected changes in temperature and precipitation in Norway range from 1.2 °C to 2.8 °C and from -1 % to 9 % in the future period 2071–2100 relative to the reference period 1991–2020.

278

279

280

281

282

283

284

285

286

The selected GCM-RCM combinations vary in data coverage and quality (Table 1). The GCM HadGEM2-ES lacks 13 months towards the end of the time series, so we only used the simulations forced by this GCM until the end of 2098. When looking at near (2041–2070) and far future (2071–2100) changes, the HadGEM2-ES simulations were shifted by two years, i.e. the periods for HadGEM2-ES were 2039–2068 and 2069–2098. In addition, HadGEM2-ES driven EURO-CORDEX CMIP5 simulations use the HadGEM2-ES calendar with 360 days instead of 365 (366) days. To fill in the missing five days, we simply copied the day number 150, 210, 240, 300 and 360 from the 360-day year and added these extra days to the day number 151, 212, 243, 304 and 365 in a normal year. For a leap year, a copy of day number 59 was added similarly. This simple technique was also used on NorESM1-M coupled with RCA4 as this model combination does not support leap years. Unrealistically large snow accumulation at isolated grid cells have been discovered in the simulations from RCA4 and HIRHAM5. They were

287 considered as minor quality issues and their effects were reduced by applying a spatial smoothing on the variables minimum,
288 mean and maximum temperature, and humidity, an approach adopted from CH2018 (2018).

289 The selection criteria for the EURO-CORDEX CMIP6 projections are different from the ones for the EURO-CORDEX CMIP5
290 projections, because there were (only) 14 RCM simulations based on CMIP6 available by June 2024 (Table S1 in
291 Supplementary material). Also, a selection of CMIP6 GCMs providing a satisfactory performance over Europe and covering
292 a reasonable part of the climate change signal had already been carried out for the EURO-CORDEX CMIP6 simulations by
293 Sobolowski et al. (2025). The main criteria for the selection here were thus to include as many GCMs as possible, a balanced
294 RCM selection and excluding model combinations that show fairly similar results in temperature and precipitation over
295 Norway. This led us to exclude the model combinations ecearthveg_rli1p1fl_icon, ecearthveg_rli1p1fl_racmo and
296 miroc_rli1p1fl_hclim. We further excluded noresm_rli1p1fl_racmo due to a low climate sensitivity and small precipitation
297 changes during the summer months.

298 **5 Downscaling and bias-adjustment methods**

299 For CiN-2015, only daily mean temperature and precipitation were bias-adjusted, but for CiN-2025, nine surface variables
300 from the RCM outputs were downscaled and bias-adjusted, namely mean, minimum and maximum air temperature at two
301 meters height, precipitation, mean wind speed at 10 meters height, long- and shortwave radiation, surface pressure, and relative
302 humidity at two meters height.

303 The nine climate variables from the RCM outputs were firstly re-gridded to the seNorge grid with a 1 km spatial resolution
304 using the nearest-neighbour method. This conservative way to downscale from a coarse to fine scale grid ensures that the
305 original model outputs are preserved and not altered unintentionally by the downscaling step. The bias-adjustment procedure
306 was then implemented on the grid cell basis. Depending on the variable adjusted, different reference datasets (see Section 2.2)
307 were used for training.

308 Since the grid cells are bias-adjusted individually, we need to select methods that are computational efficient, or at least
309 applicable, and numerically stable (François et al., 2020) for a large number of grid cells (354 448 in total). We have tested a
310 few bias-adjustment techniques categorized as quantile mapping (Cannon et al., 2015) and multivariate approaches (François
311 et al., 2020). In the end, the univariate bias-adjustment adopting de-trended empirical quantile mapping (EQM) approach
312 (Bürger et al., 2013) was used to bias-adjust one climate variable at a time because the method meets all the aforementioned
313 criteria and is widely used in adjusting climate model data. EQM is effective in removing the model biases, preserving the
314 trend and climate change signal moments (i.e. mean and standard deviation) and estimating extremes. As no univariate method
315 can correct the possible biases in correlation among the atmospheric variables, all the EQM results were further post-processed

316 with the multivariate 3DBC approach (Mehrotra and Sharma, 2019) to rectify inter-variable, temporal and spatial dependency
317 structures.

318 **5.1 EQM**

319 The EQM approach adopted in this study is a de-trended variant of quantile mapping method which first establishes a statistical
320 transfer function for a variable between RCM outputs and reference data in the training period 1985–2014. Twelve calendar-
321 month-specific transfer functions were derived by fitting the empirical cumulative distribution functions (eCDFs) of the
322 modelled values with the eCDFs based on reference data for each grid cell. With these monthly bias-adjustments we correct
323 model biases which are varying throughout the year. This is essential for instance to produce realistic seasonal flow patterns
324 and hydrological regimes in the subsequent hydrological modelling. To avoid overfitting, daily data within a 3-month window
325 centred on the month of interest were pooled and used to develop the monthly eCDFs (Cannon et al., 2015). For example, data
326 from February to April were used to develop the eCDF for March.

327 The transfer functions were approximated by a series of empirical quantiles with fixed intervals of 0.01 spanning the probability
328 space (0,1) (Gudmundsson et al., 2012). Only the 1st to 99th quantiles were obtained and used. Linear interpolation was applied
329 for values in between those fixed quantiles. For values smaller than the 1st quantile and larger than the 99th quantile, linear
330 extrapolation was performed based on the slopes derived from the 1st and 2nd quantiles and 98th and 99th quantiles
331 respectively. These functions are assumed to be applicable to the projection period.

332 Wet-day correction has also been applied prior to bias-adjustment of precipitation because RCMs generally provide more rainy
333 days than the observed ones (Frei et al., 2003). For each grid cell, a threshold value is derived such that the wet-day frequency
334 in modelled precipitation is equal to that in the corresponding reference data for the training period. All modelled precipitation
335 values which are below the derived threshold value are then set to zero for both training and projection periods (Gudmundsson
336 et al., 2012).

337 To reduce the potential impact of over-adjustment (modifying the long-term linear trend) and extrapolation (model-projected
338 values lying outside the range of the historical distribution), the long-term linear trend (usually 30-year) of the projected period
339 was first removed from model projections. This shifting of the future distribution can better secure the applicability of the
340 transfer function based on historical distribution. And the daily variability about the monthly mean remained unchanged. The
341 trend was later reimposed after the bias-adjustment of the ‘residuals’. For all the variables other than temperatures, trend
342 removal and reimposition were performed multiplicatively. For example, relative trend for precipitation for month i , δP_i , is
343 defined as:

$$344 \delta P_i = \bar{P}_i^{prj} / \bar{P}_i^{tnq} \quad (1)$$

345 where \bar{P}_i^{prj} and \bar{P}_i^{tnq} refer to mean monthly accumulated precipitation for month i for the projection and training periods,
 346 respectively. The de-trended (normalized) daily precipitation, \hat{P}_{ij}^{prj} , for month i and day number j in the projection period is:

$$347 \quad \hat{P}_{ij}^{prj} = P_{ij}^{prj} / \delta P_i \quad (2)$$

348 where P_{ij}^{prj} denotes the original RCM daily precipitation for month i and day number j in the projection period. EQM was then
 349 applied to the ‘normalized’ time series, and the precipitation trend for month i was then re-introduced to the bias-adjusted
 350 normalized results \check{P}_{ij}^{prj} for month i and day number j . The bias-adjusted precipitation, \tilde{P}_{ij}^{prj} , for month i and day number j can
 351 be obtained by:

$$352 \quad \tilde{P}_{ij}^{prj} = \check{P}_{ij}^{prj} \cdot \delta P_i \quad (3)$$

353 Similarly linear trend removal and reimposition for the projected values of temperature variables were done additively.
 354 Following similar notation, the temperature trend, δT_i , for month i simply equals to $\bar{T}_i^{prj} - \bar{T}_i^{tnq}$, and the de-trended (residual)
 355 daily temperature, \hat{T}_{ij}^{prj} , can be derived from:

$$356 \quad \hat{T}_{ij}^{prj} = T_{ij}^{prj} - \delta T_i \quad (4)$$

357 where T_{ij}^{prj} represents the original RCM daily temperature for month i and day number j in the projection period. The bias-
 358 adjusted temperature for month i and day number j , \tilde{T}_{ij}^{prj} , can be recovered by adding the temperature trend δT_i to the bias-
 359 adjusted residual data \check{T}_{ij}^{prj} :

$$360 \quad \tilde{T}_{ij}^{prj} = \check{T}_{ij}^{prj} + \delta T_i \quad (5)$$

361 The projection period starting from 2015 to 2100 was further divided into seven overlapping 30-year time slices. The first time
 362 slice, however, only covers 2015-2040, followed by 2021-2050, 2031-2060, etc. After the bias-adjustment of each time slice
 363 using the established monthly transfer functions, only the 10-year results in the middle of the period were being kept. This
 364 procedure can better preserve the decadal trend. For the first and the last time slices, the results of the first 16 years and the
 365 last 20 years were used respectively. A continuous time series covering the whole projection period was put together
 366 afterwards.

367 **5.2 3DBC**

368 The bias-adjusted climate projections based on the univariate EQM approach show the same dependency structures as the
 369 uncorrected RCM simulations. To impose inter-variable, temporal and spatial dependency structures obtained from the
 370 reference datasets, an additional post-processing step has been applied. The multivariate method we used for this is called
 371 3DBC (three-dimensional bias-correction) as it adjusts along the three dimensions: variables, time and space. It is described

372 in detail in Mehrotra and Sharma (2019). 3DBC is re-establishing the spatial, temporal and inter-variable structures from the
 373 reference data by reordering the daily EQM values according to observed time-ranks at each grid-point, resulting in the bias-
 374 adjusted data having the same rank structure (ordering) as the reference data in the calibration period. Compared to other
 375 multivariate bias correction methods (e.g. the MBCn method developed by Cannon, 2018) the computational requirements of
 376 3DBC are relatively small, making its application on a large number of grid cells feasible. Note that 3DBC adjusts the ranks
 377 for future periods according to changes in the temporal auto-correlations as simulated by the RCMs. Thus, it does not strictly
 378 assume that the dependency structures remain stable in future climates. However, while the original implementation by
 379 Mehrotra and Sharma (2019) works on single calendar days across a future period of 30 years, our future period (2021-2100)
 380 consists of 80 years. Following the original approach would have resulted in imposing observed trends repeatedly on the future
 381 period. We thus adapted the 3DBC method to work within single years of the EQM data, an approach that maintains the climate
 382 change signals and trends from the RCMs (and EQM) on an annual scale. As a result, the adjustments in the variable auto-
 383 correlations for the future periods have a limited effect and do not fully transfer the dependency structure changes from the
 384 RCMs to the 3DBC bias-adjusted data. Since 3DBC reshuffles the bias-adjusted times series resulting from EQM within a
 385 year, the marginal distributions at seasonal scale might be modified.

386 **5.3 Evaluation of bias-adjustment methods**

387 **5.3.1 Performance of bias-adjustment methods**

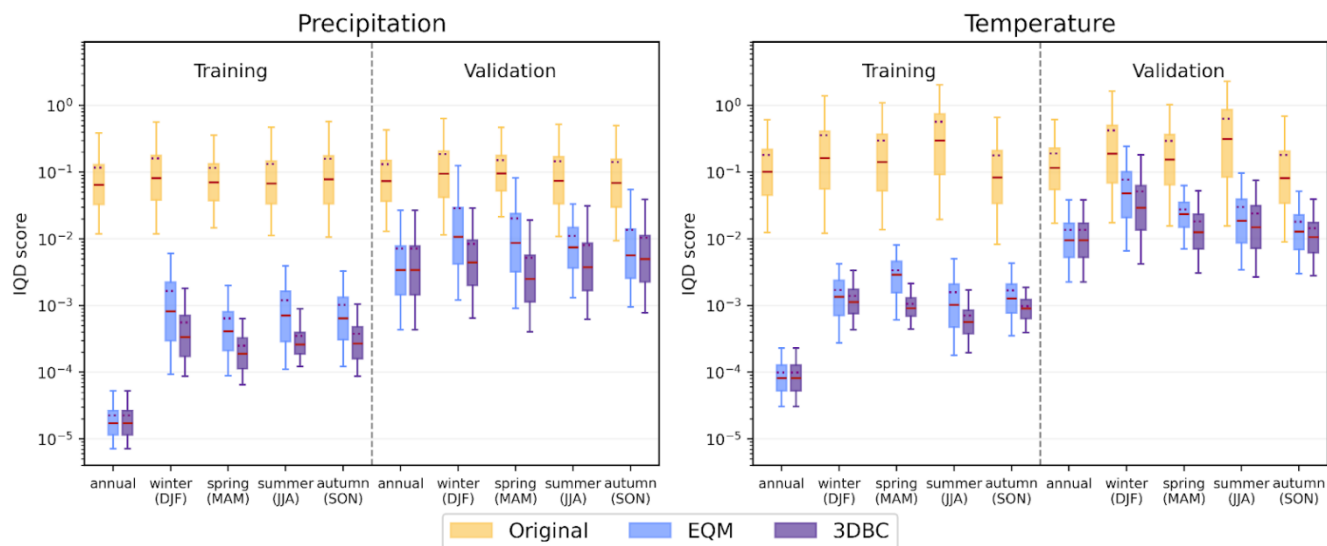
388 Thorarinsdottir et al. (2013) proposed the use of integrated quadratic distance (IQD) as a performance measure to compare the
 389 full distribution of climate model output to the corresponding distribution of observed data. IQD was further employed by
 390 Yuan et al. (2019; 2021) to assess the performance of different bias-adjustment approaches. IQD (Eq. 6) is defined as:

$$391 \quad d_{IQ}(F, G) = \int_{-\infty}^{+\infty} (F(t) - G(t))^2 dt \quad (6)$$

392 where F , G are two cumulative distribution functions. $d_{IQ}(F, G)$ summarizes the differences, and a lower value implies a
 393 smaller difference between F and G . $d_{IQ}(F, G) = 0$ if $F = G$. For further details, please see Thorarinsdottir et al. (2013). In this
 394 study, we compared the eCDFs of bias-adjusted precipitation and temperature with corresponding seNorge2018 v20.05 data
 395 over the training (1985–2014) and validation (1960–1984 or 1970–1984 depending on the period start of the RCM) periods
 396 in each grid cell. In addition, we calculated IQD scores derived from comparison of original RCM outputs with the observed
 397 data.

398 IQD scores for precipitation and temperature are presented in Fig. 4. The results clearly demonstrate that both bias-adjustment
 399 approaches are far better at reproducing the full distributions of observed precipitation and temperature by several orders of
 400 magnitude than the original RCM outputs. As expected, the improvements are larger (smaller d_{IQ}) in the training period than
 401 the validation period. EQM and 3DBC have the same performance on annual results, but 3DBC generally performs better than

EQM on seasonal results because 3DBC utilizes additional information about the intra-annual order of the observed time series in the post-processing. The only exceptions are the IQD scores from particular RCMs (CCLM4-8-17, REMO2015 and REMO2009), which show that EQM provides marginally better results than 3DBC in autumn (Fig. S1 in Supplementary materials). It might indicate that the observed ranks in autumn of the training and validation periods are quite different and that those models partly capture this change. Overall, 3DBC provides added value as compared to EQM when seasonal statistical properties are of importance.

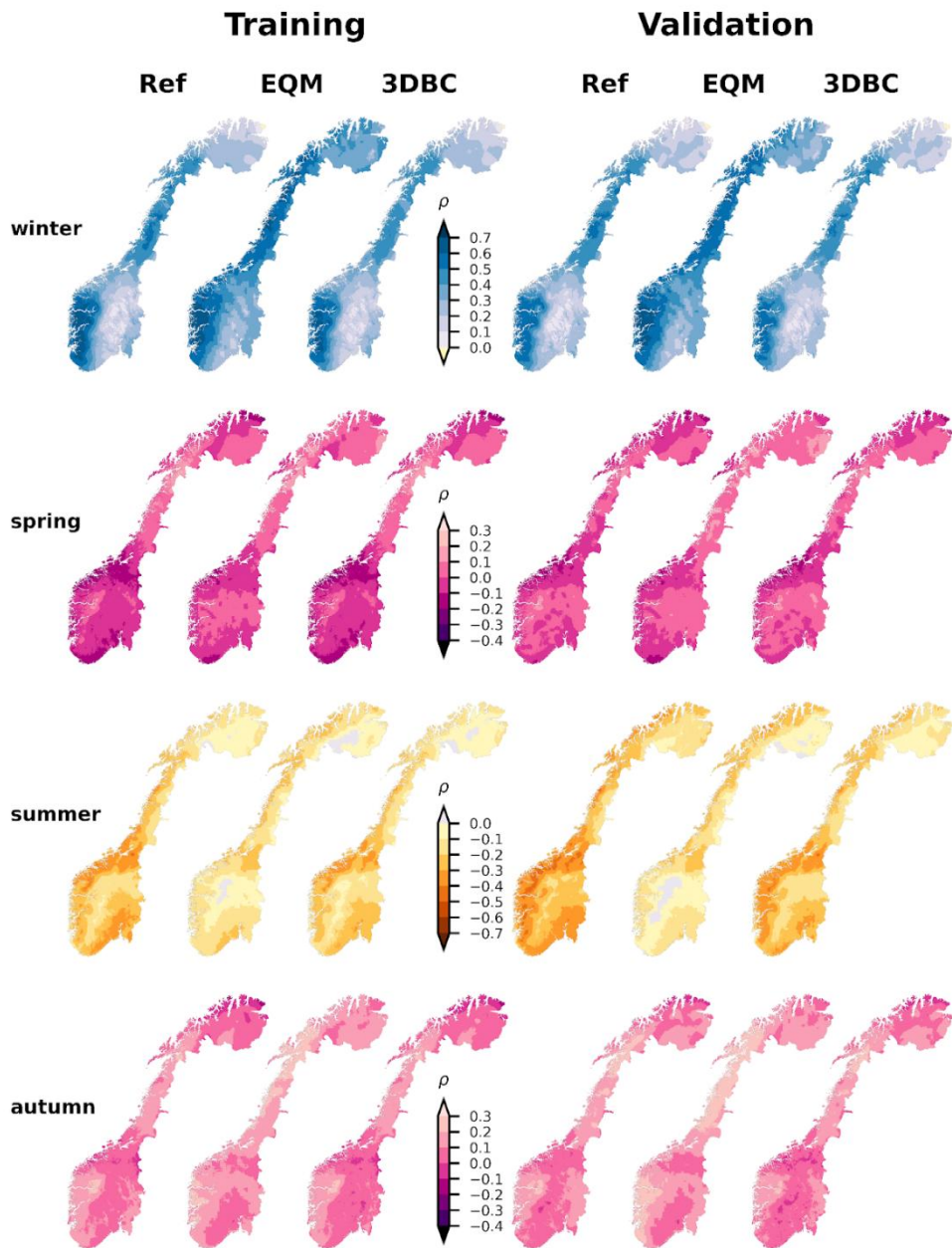


408

409 **Figure 4: Integrated quadratic distance (IQD) scores for precipitation (left panel) and temperature (right panel) based**
 410 **on the CMIP5 model ensemble. Bias-adjusted results from EQM and 3DBC in addition to the original model outputs**
 411 **are compared with the reference datasets seNorge2018 v20.05 over the training (1985–2014) and validation (1960/70–**
 412 **1984) periods. The red line on the box indicates the median value whilst the dotted line represents the mean. The lower**
 413 **and upper boundaries of the box are the 25th and 75th percentiles. The lower and upper ends of the whiskers refer to**
 414 **the 5th and 95th percentiles.**

Besides the seasonal statistics, 3DBC can simulate better spatial correlation structures between precipitation and temperature in the historical period than EQM, as it reorders the modelled ranks of precipitation and temperature based on observations while the univariate EQM method keeps the spatial rank correlation pattern from the RCM. Figure 5 shows an example of the spatial distribution of seasonal Spearman’s rank correlation coefficient (ρ), calculated based on the bias-adjusted datasets from EQM and 3DBC and the reference datasets for training (1985–2014) and validation (1960–1984) periods for one RCM. In general, ρ are largest and positive in winter (warm days are wetter), followed by negative ρ in summer (warm days are dry, cold are wet). In spring and autumn, ρ is much smaller than in summer and winter, indicating a rather weak rank correlation

422 between precipitation and temperature. The differences in the spatial correlation structure between these two methods are often
423 most pronounced in winter and summer. EQM usually overestimates the positive rank correlations almost over the whole
424 country in winter, whilst it underestimates negative dependencies in summer. And this spatial rank correlation pattern seems
425 to be rather stable from one period to another. Aggregated results for each model combination are shown as boxplots (Fig. S2
426 in Supplementary materials), and they confirm that 3DBC performs better in recovering the inter-variable spatial dependency
427 structure for all RCMs.



428

429

430

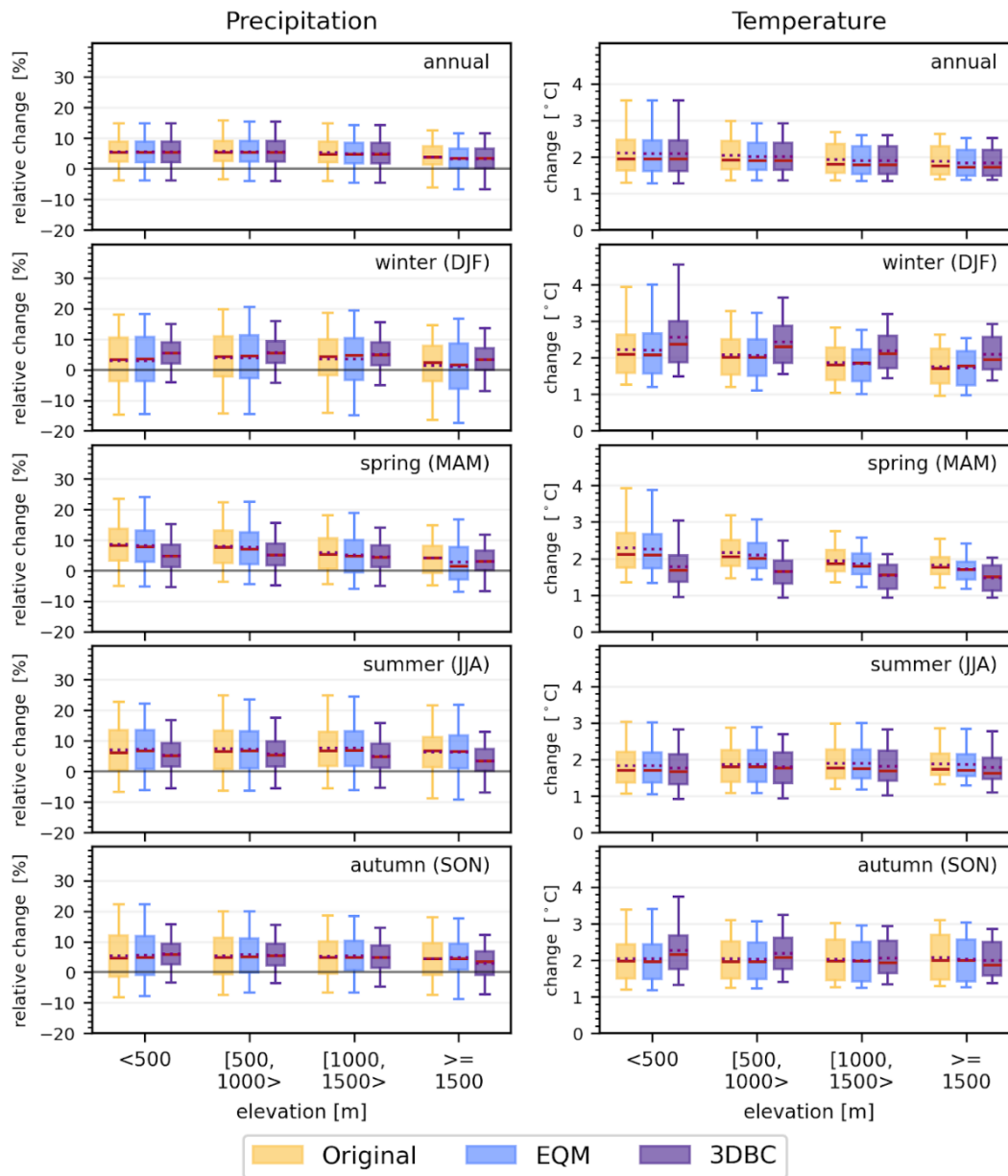
431

432

Figure 5: Spatial distribution of Spearman's rank correlation coefficient ρ of daily precipitation and temperature in winter (DJF), spring (MAM), summer (JJA) and autumn (SON) for the two bias-adjustment methods. For training (1985–2014) and validation (1960–1984) periods, the two bias-adjusted datasets, EQM and 3DBC are based on historical run from CMIP5-based mpi-r11p1-ccsm and compared with reference datasets seNorge2018 v20.05.

433 5.3.2 Climate change signal preservation

434 The two bias-adjustment methods can lead to different climate change signals in the future periods (e.g. 2071-2100) relative
435 to the reference period (1991-2020). Figure 6 shows the annual and seasonal changes grouped in four elevation bands (< 500,
436 [500, 1000>, [1000,1500>, > 1500), including 52%, 32.7%, 13.6% and 1.7% of the grid cells in Norway, respectively. The
437 result aligns with other recent studies demonstrating that the change signals are elevation-dependent (Astagneau et al.,2025,
438 Matiu et al., 2024). The two bias-adjustment methods provide identical annual climate change signals, since 3DBC uses the
439 same bias-adjusted results from EQM before further post-processing. EQM generally preserves the seasonal climate change
440 signals from the original RCMs in terms of both mean and median changes as well as the spread of changes for all elevation
441 bands. However, by reshuffling the chronological order intra-annually, 3DBC modifies the seasonal change signals from the
442 original RCMs, leading to larger increases in precipitation and temperature in winter and smaller increases in spring than the
443 original RCM outputs. In summer and autumn, the climate change signals can be underestimated or overestimated by 3DBC
444 depending on the variables and elevations.



445

446 **Figure 6: Projected annual and seasonal changes in precipitation (relative change in %, left column) and temperature (change in**
 447 **°C, right column) from 1991–2020 to 2071–2100 for RCP4.5 in terms of elevation. Results grouped in four elevation bands from two**
 448 **bias-adjustment procedures, EQM and 3DBC, are compared to the original RCM projections. The red line on the box indicates the**
 449 **median value whilst the dotted line represents the mean. The lower and upper boundaries of the box are the 25th and 75th percentiles.**
 450 **The lower and upper ends of the whiskers refer to the 5th and 95th percentiles.**

451 **6 Hydrological modelling**

452 **6.1 distHBV**

453 distHBV is a spatially distributed version of the HBV precipitation-runoff model (Beldring et al., 2003) and is the major tool
454 applied to assess hydrological responses to climate change in Norway. The model calculates the water balance for 1 x 1 km
455 grid cells at a daily time step covering the entire mainland surface area of Norway and upstream areas in Finland and Sweden
456 contributing to streamflow in Norwegian catchments. Each grid cell includes one soil type and up to five land cover types.
457 distHBV has components for accumulation, sub-grid scale distribution and ablation of snow, interception storage, sub-grid
458 scale distribution of soil moisture storage, evapotranspiration, groundwater storage and runoff response, lake evaporation and
459 glacier mass balance. The newly implemented Penman-Monteith method and the prescribed parameterizations are presented
460 in Huang et al. (2019) and Erlandsen et al. (2021).

461 As for other conceptual hydrological models, calibration is necessary to adjust the distHBV parameters to improve the model
462 performance of reproducing observed discharge, due to the absence of directly measured catchment characteristics, natural
463 variability and the non-linearity of the processes involved. Since all parameters to calculate potential evaporation are prescribed
464 in the Penman-Monteith equation, the calibration parameters are mainly associated with lake, subsurface, snow and glacier
465 processes (Table 2). Different from the lumped version of HBV, the parameters associated with snow and subsurface processes
466 in distHBV vary by land cover type (deciduous forest, coniferous forest and others) and soil-type (the five soil types based on
467 the sediment map (Section 2.3) plus glacier bed), respectively. In total, there are 44 parameters for modelling mainland of
468 Norway, including six snow parameters (two snow parameters times three land use classes), 36 soil parameters (six soil types
469 times six subsurface parameters) and two parameters associated with lake and glacier processes. The parameters vary between
470 grid cells due to different combinations of soil and land cover types within grid cells. Note that we didn't distinguish the snow
471 parameters for all land cover types because it will increase equifinality risks due to too many calibration parameters and forest
472 is one of the dominant land cover types in Norway (Huang et al., 2026). In addition, we didn't calibrate the rainfall or snow
473 correction parameters as in other HBV applications, because it will lead to inconsistency between the climate and hydrological
474 projections in terms of water balance.

475 **Table 2: list of calibration parameters. Note that the parameters associated with the snow and subsurface processes vary by land**
476 **cover and soil type, respectively.**

477

Associated process	Parameter	Explanation	Unit	Min	Max
Lake	KLAKE	Rating curve constant	-	1.00E-04	0.1
Snow and glacier	SMELT_T	Snow melt temperature	°C	-1	2
	SMELTR	Temperature index for snow melt rate	m/°C	1.00E-04	0.01
	IMELTR	Ice melt rate for glaciers additional coefficient to SMELTR	-	1	4
	FC	Field capacity	m	1.00E-02	1
Subsurface	BETA	Shape coefficient of soil moisture	-	1	5
	KUZ	Upper zone recession coefficient	-	1.00E-03	1
	ALFA	Upper zone nonlinear drainage coefficient	-	1	2
	PERC	Percolation from upper zone to lower zone	-	1.00E-03	0.5
	KLZ	Lower recession coefficient	-	1.00E-03	1

478

479

480

481

482

483

484

The model was calibrated against discharges at 85 gauges (Fig. 1) from 2000 to 2007 using the parameter estimation routine PEST (Doherty and Skahill, 2006) and a multi-criteria calibration approach (Huang et al., 2019). The multi-criteria include the Nash and Sutcliffe efficiency (NSE) (Nash and Sutcliffe, 1970), the bias in water balance (BIAS) and the volume bias in the high-flow segment of the flow duration curve (ΔFHV , 0 – 0.02 flow exceedance probabilities) (Yilmaz et al., 2008). Since PEST minimizes the difference between the criteria results and their ideal values (1 for NSE and 0 for biases), the calibration objective function θ containing the three criteria at multiple gauges can be formulated as Eq. 7.

485

$$\theta = W_{NSE} * \sum_{i=1}^n (1 - NSE_i)^2 + W_{BIAS} * \sum_{i=1}^n (BIAS_i)^2 + W_{\Delta FHV} * \sum_{i=1}^n (\Delta FHV_i)^2 \quad (7)$$

486

487

where W are weights for each criterion and $n = 85$, the number of calibration catchments. W_{NSE} equals to 8 and W_{BIAS} and $W_{\Delta FHV}$ equal to 1 to achieve a good calibration performance.

488

489

490

491

492

493

494

Five PEST runs were carried out with different initial parameter values and only the parameter set giving the best model performance was selected for model validation. The model was validated against the discharge of the 85 calibration stations and additional 38 gauging stations from 2011 to 2020 to evaluate the temporal and spatial transferability of the model, respectively. The validation period (2011 – 2020) was selected because it is the warmest period for most catchments in the recent decades. Compared to the calibration period (2000 – 2007), the average increase in annual mean temperature of all 123 catchments is about 0.43 degrees in 2011 – 2020. Hence, the validation results show the model performance under warmer conditions.

495

496

497

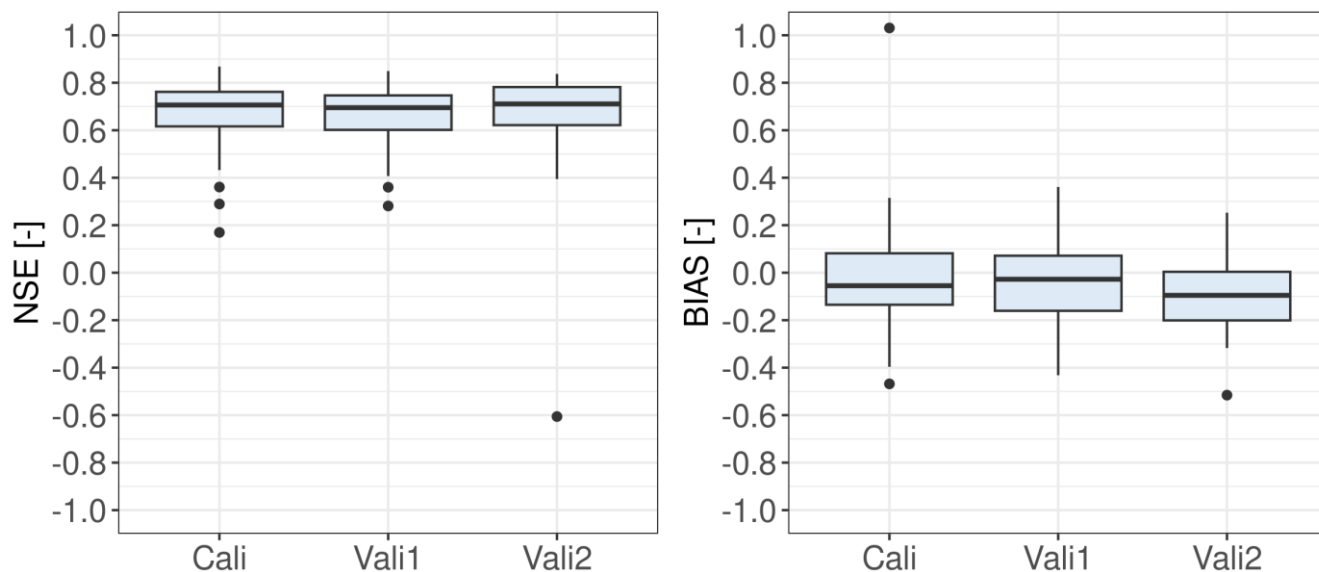
498

499

500

Figure 7 shows the calibration and validation results in terms of NSE and BIAS. During the calibration period, about 50% and 29% of the catchments show good ($NSE > 0.65$ and $|BIAS| < 0.1$) and satisfactory ($0.65 > NSE > 0.55$ and $0.1 < |BIAS| < 0.15$) results (Moriiasi et al., 2007), respectively. The model generally underestimates discharge with the median bias of -5%, mainly due to underestimation of precipitation in seNorge2018 v20.05 data. The model performs similarly in terms of NSE in the validation period for the 85 gauging stations, with the median NSE degraded by only 0.01. The median bias is reduced by 0.025 in the validation period than in the calibration period but there are more catchments with $|BIAS| > 0.1$. The model performance varies

501 with time, partly due to parameter transferability problems under different climate conditions and partly due to the quality of
 502 seNorge2018 v20.05 dataset that also varies with time (Lussana et al., 2019; 2020). The validation results for the additional
 503 38 gauging stations show robust spatial transferability of the model, with good or satisfactory ($NSE > 0.55$ and $|BIAS| < 0.15$)
 504 model performance for about 58% of the catchments. The model generally underestimates discharge with BIAS less than -0.1
 505 for about half of the validation gauging stations. Such calibration and validation results are acceptable with consideration of
 506 the quality of the meteorological forcing data in such a mountainous region and simultaneous calibration for all catchments.



507
 508 **Figure 7: distHBV model performance in terms of NSE and BIAS for the 85 calibration catchments in the calibration period 2000 –**
 509 **2007 (Cali), for the 85 calibration catchments in the validation period 2011 – 2020 (Vali1) and for the 38 validation catchments in**
 510 **the validation period 2011 – 2020 (Vali2).**

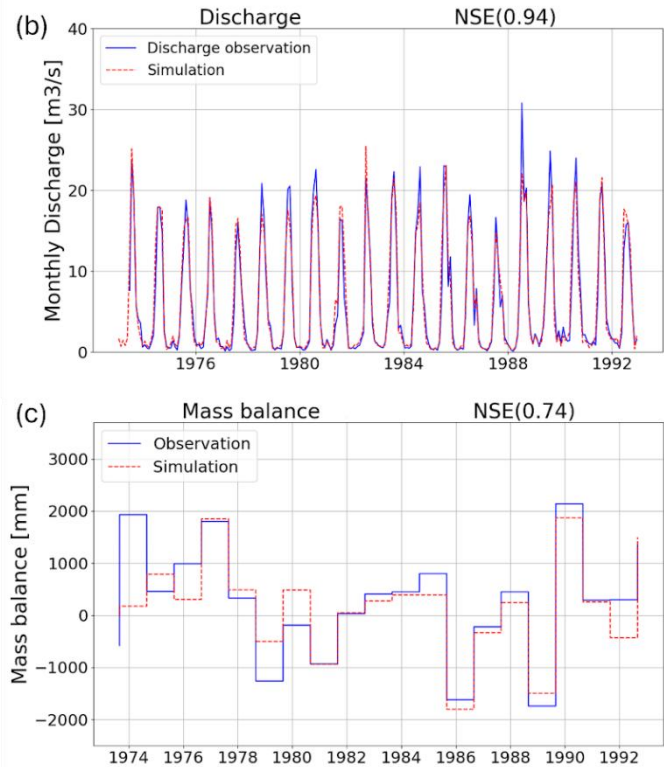
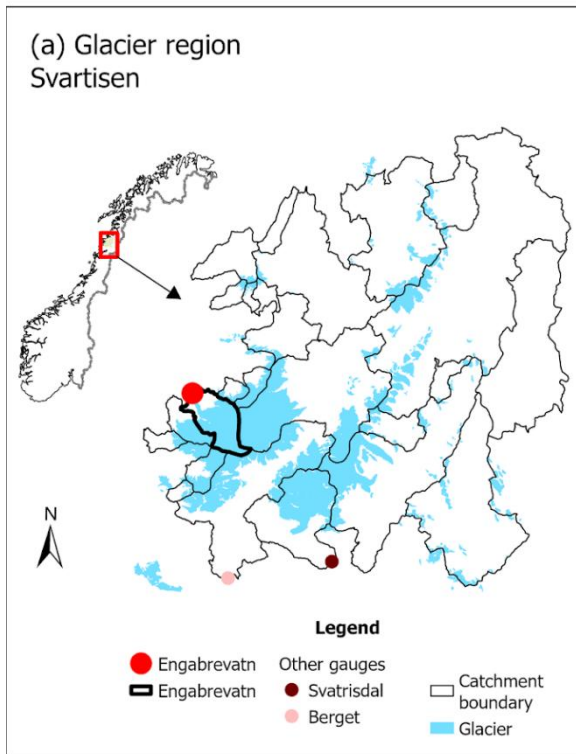
511 **6.2 DEW**

512 Distributed Element Water balance model (DEW) hydrological model (Beldring, 2008; Li et al., 2015) was used to simulate
 513 climate change impacts on glaciers for 12 given glacier regions in Norway. The smallest glaciers ($< 1 \text{ km}^2$) were omitted in
 514 the DEW model. This model differs from distHBV in the respect that it also calculates changes in glacier ice area, volume and
 515 surface elevation, and water balance. In addition, the model requires additional information as input, such as ice thickness and
 516 glacier area for grid cells with glaciers. However, DEW uses only daily mean temperature and precipitation as meteorological
 517 forcing data as it uses a temperature-based degree-day model to estimate potential evapotranspiration.

518 Snow and glacier ice melt were calculated using a degree-day model, with different degree-day factors for snow and ice. DEW
519 applies a simplified model called DeltaH (Huss et al., 2010) to describe the changes in glacier ice area, volume and surface
520 elevation. The method simulates the impacts of ice movement that transports mass from the highest to the lowest areas of the
521 glacier. Simulations without taking this redistribution of glacier ice into account will give incorrect estimates for both glacier
522 changes and the water flow from the glacier. It is based on historically observed elevation changes of the glacier surface
523 elevation and how these are distributed over the glacier area. The pattern of change is then used when simulating the
524 development of glacier ice area, volume and surface elevation under climate scenarios by having the model redistribute mass
525 over the glacier at the end of each mass balance year. Ice melt caused by negative mass balance results in diminishing of the
526 glacier ablation area. Simulations with more advanced, physically based glacier models that simulate the flow of ice in the
527 glaciers would probably be more realistic but are more demanding to run and require much more input data that are not
528 available for most glacier areas in Norway.

529 DEW was calibrated using the same parameter estimation routine (PEST) as used for distHBV, but it was calibrated against
530 observed daily streamflow and annual mass balance data for six out of the 12 glacier regions. Within each of the six regions,
531 one optimal model parameter set was determined for all glaciers and catchments. This strategy was chosen to avoid
532 discontinuities in model results between or along catchment boundaries and ice divides. Fixed periods were not used for
533 calibration and validation as in the case of distHBV, because the availability of observed data varied both in time and space.
534 It was a challenge to find both mass balance and streamflow time series of good quality at the same period, leading to limited
535 time series available for model validation in some cases. During model calibration, mean NSE value is 0.75 for daily discharge
536 of 19 gauging stations downstream of the glaciers, and 0.72 for annual mass balance for six glaciers. The mean NSE value for
537 daily discharge during model validation is 0.74. For the remaining six glacier regions where there were no streamflow data
538 available, model parameters were transferred from the nearest glacier region with calibrated parameters.

539 Figure 8a shows one of the 12 glacier regions, called Svartisen, as an example. For this region, DEW was setup for all
540 catchments where glacier melt contributes to river discharge. Among these catchments, only three catchments (Engabrevatn,
541 Svartisdal and Berget) have discharge observations in good quality and only Engabrevatn has the measured mass balance data.
542 Based on the data availability of both discharge and mass balance data, DEW was calibrated against the discharge of the three
543 catchments and glacier mass balance in Engabrevatn for the period 1974–1993. The calibrated parameters were then
544 transferred to other catchments of this region for hydrological projections. Figure 8b and 8c compare the observed and
545 simulated discharge and mass balance for Engabrevatn in the calibration period. It shows that the model can well reproduce
546 both monthly discharge and annual glacier mass balance with NSE larger than 0.7.



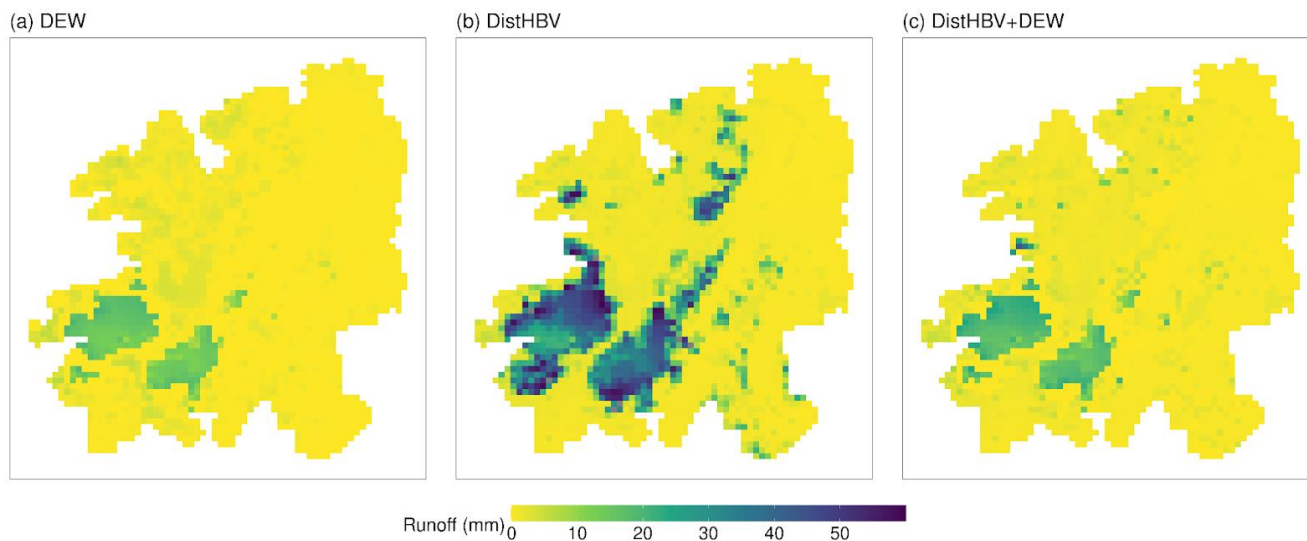
547

548 **Figure 8: The glacier region Svartisen (a), observed and simulated discharge (b) and annual mass balance (c) for the catchment**
 549 **Engabrevatn.**

550 6.3 Postprocessing of distHBV and DEW outputs

551 The final runoff projections for mainland Norway were produced by replacing distHBV outputs with the DEW ones. Note that
 552 DEW simulated the whole glacierized catchments (Fig. 8a) but only the outputs for the grid cells with glaciers were used to
 553 replace the distHBV results. It is mainly because DEW uses a simpler potential evapotranspiration (PET) method and rougher
 554 landuse/soil classes than distHBV. Figure 9 (a and b) shows the simulated runoff projections using DEW and distHBV for the
 555 glacier region Svartisen (Fig. 8a) on 31st August 2100 driven by the ecearth-r12i1p1-clm climate projection. Without
 556 considering glacier retreat, distHBV projected high runoff (> 20 mm) for most grid cells where glaciers exist at present while
 557 DEW projected much lower runoff for these grid cells than distHBV, confirming that distHBV overestimates runoff under
 558 warming conditions. After we replaced the distHBV results with the DEW ones, the final output is more reasonable for this
 559 region than the distHBV one (Fig. 9c). Note that there are still single grid cells with high runoff in the final product because
 560 of different glacier masks used by DEW and distHBV. In addition, small glaciers outside the glacierized catchments (Fig. 8a)

561 were not simulated by the DEW model and the results for these small glaciers cannot be corrected.



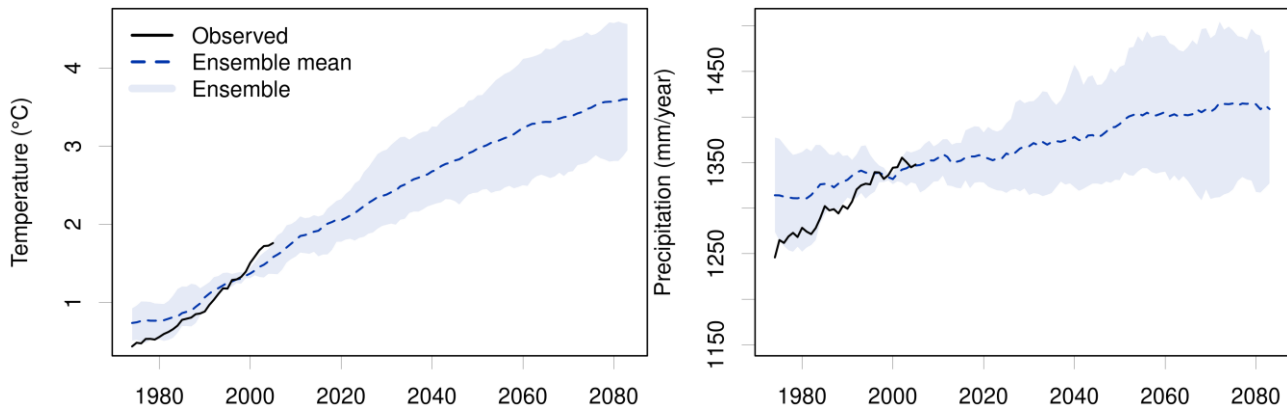
562

563 **Figure 9: Simulated runoff on 31st August 2100 for the glacier region Svartisen by DEW (a), distHBV (b) and the combination of**
564 **distHBV and DEW (c) driven by the ecearth-r12i1p1-clm climate projection.**

565 7 National climate projections

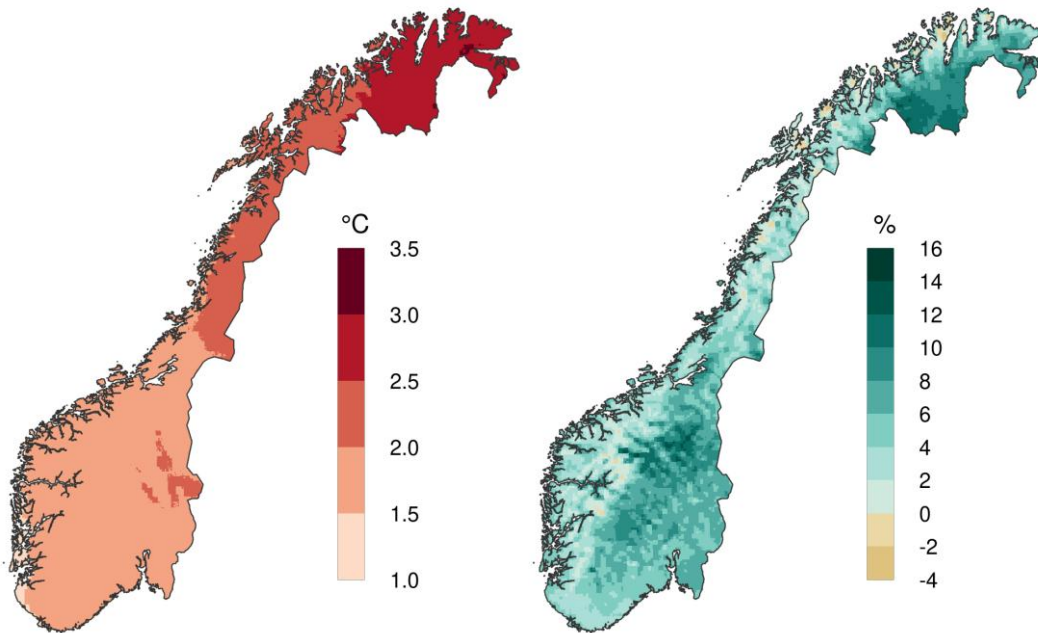
566 7.1 Ensemble means and ranges

567 There are 20 climate projections for mainland Norway at 1km spatial resolution with daily time steps under the RCP4.5
568 scenario from the COR-BA-2025 dataset. Figure 10 shows 30-year running means of annual temperature and precipitation
569 sums from 1971 to 2098 for Norway. There is a clear increase in temperatures visible in the mean and the whole ensemble.
570 For precipitation, the ensemble mean is also increasing but the lower limit of the projection ensemble is showing a stable
571 precipitation amount of about 1325 mm/year. The observed historical values are mostly within the simulated precipitation and
572 temperature ensembles but are located at the lower end of the ensemble before the year 2000 and at the upper end afterwards,
573 indicating that the RCP4.5 ensemble underestimates recent temperature and precipitation trends in Norway. Note that all RCMs
574 are bias-adjusted to match the observed values averaged over the training-period 1985-2014 and the spread in the ensemble
575 equals zero for the middle of that period (year 2000). In addition, the ensemble spread is exactly the same for both EQM and
576 3DBC methods as 3DBC has the same change statistics as EQM on an annual basis.



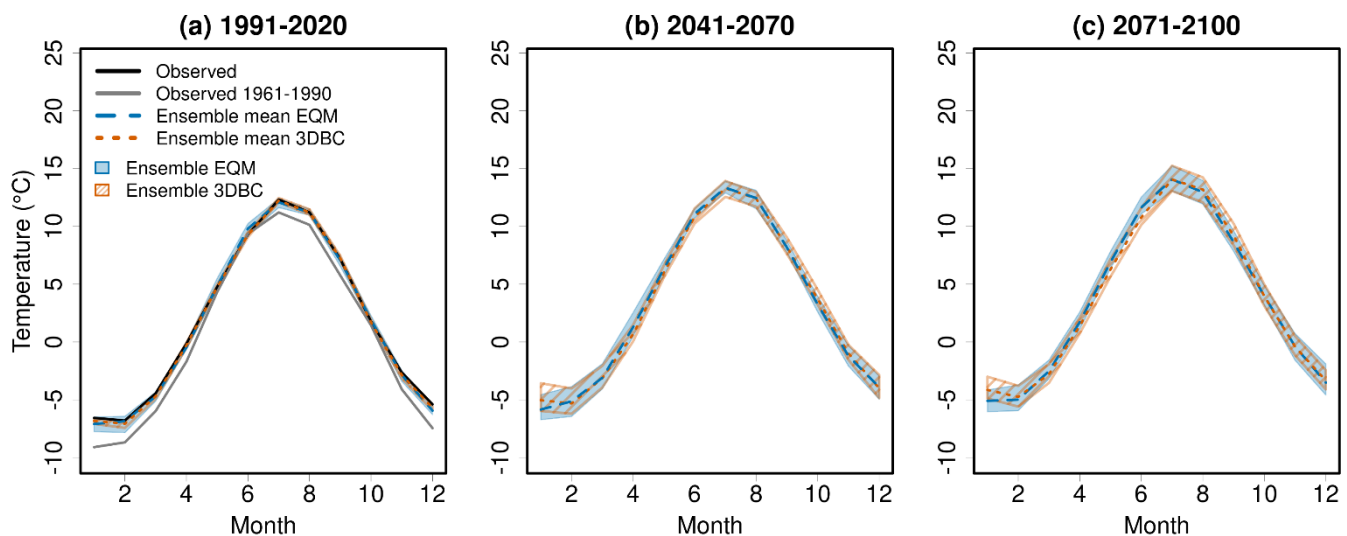
577
 578 **Figure 10: Simulated 30-year running means of temperature (left) and precipitation (right) from the COR-BA-2025 ensemble of 20**
 579 **climate projections (10 GCM-RCM combinations x 2 bias-adjustment methods) for Norway under the RCP4.5 emission scenario.**

580 Looking at the spatial distribution of changes from the reference period 1991–2020 to the far future period 2071–2100 (Fig.
 581 11), a generally larger increase in temperatures towards the North is apparent, with about one to two °C in the southern and
 582 two to three °C in the northern half of Norway. Precipitation is increasing as well with exceptions of some isolated areas along
 583 the coast and in the mountains. Generally, the precipitation increases are small and below +12%.



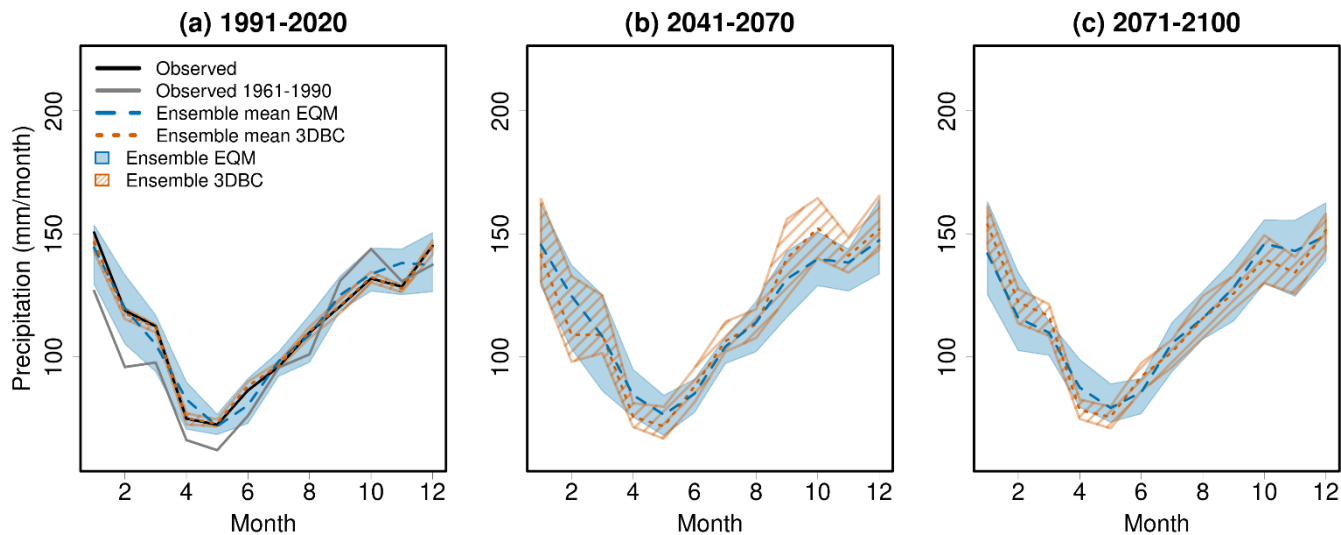
584
 585 **Figure 11: COR-BA-2025 ensemble mean changes in temperature (°C) (left) and relative changes in precipitation (%) (right) in the**
 586 **scenario period 2071–2100 relative to the reference period 1991–2020 under the RCP4.5 scenario for mainland Norway.**

588 The effects of the two bias-adjustment methods on the preservation and altering of the seasonal climate change signals of the
 589 RCMs is shown in Fig. 6 and discussed in Section 5.3.2. Similarly, the two methods have different effects on the monthly
 590 climate change signal due to their design. While EQM is designed to preserve the monthly climate change signals, the 3DBC
 591 method is designed to provide spatial, temporal and inter-variable structures based on the reference data. However, as can be
 592 seen in Fig. 12 and 13, the shapes of the climatologies from EQM and 3DBC are similar and in agreement with the observed
 593 ones. As already seen for the seasonal changes (Fig. 6), precipitation and temperature changes in 3DBC are larger than in EQM
 594 in winter months (especially January and February) and smaller in spring and summer (April to June) for the far future period
 595 (2071–2100). For the near future (2041–2070), the difference in the changes from EQM and 3DBC are less systematic but
 596 3DBC shows a pronounced increase in autumn precipitation which is absent in EQM (Fig. 13). This shift in the 3DBC results
 597 can be traced back to its implementation: the rank structure from the reference years 1961-1990 are used for the 2041-2070
 598 period. Since the autumn precipitation in the period 1961-1990 has been large (Fig. 13a), this is imprinted on the mean annual
 599 cycle of the near future period. For the current climate (1991–2020), the 3DBC method results in climatologies that are similar
 600 for all models and thus a small ensemble-spread compared to the EQM data. This is especially true for precipitation (Fig. 13).



601
 602 **Figure 12: 30-year mean monthly temperatures for Norway for different time periods using the EQM and 3DBC bias-adjusted**
 603 **climate projections under the RCP4.5 scenario. Black line: Observed temperature in 1991–2020. Grey line: Observed temperature**
 604 **in 1961-1990. Blue and orange lines: ensemble means of simulated temperature. Blue and orange striped areas: ensemble spread of**
 605 **10 projections.**

606



607
608 **Figure 13: The same as Fig. 12 but for precipitation.**

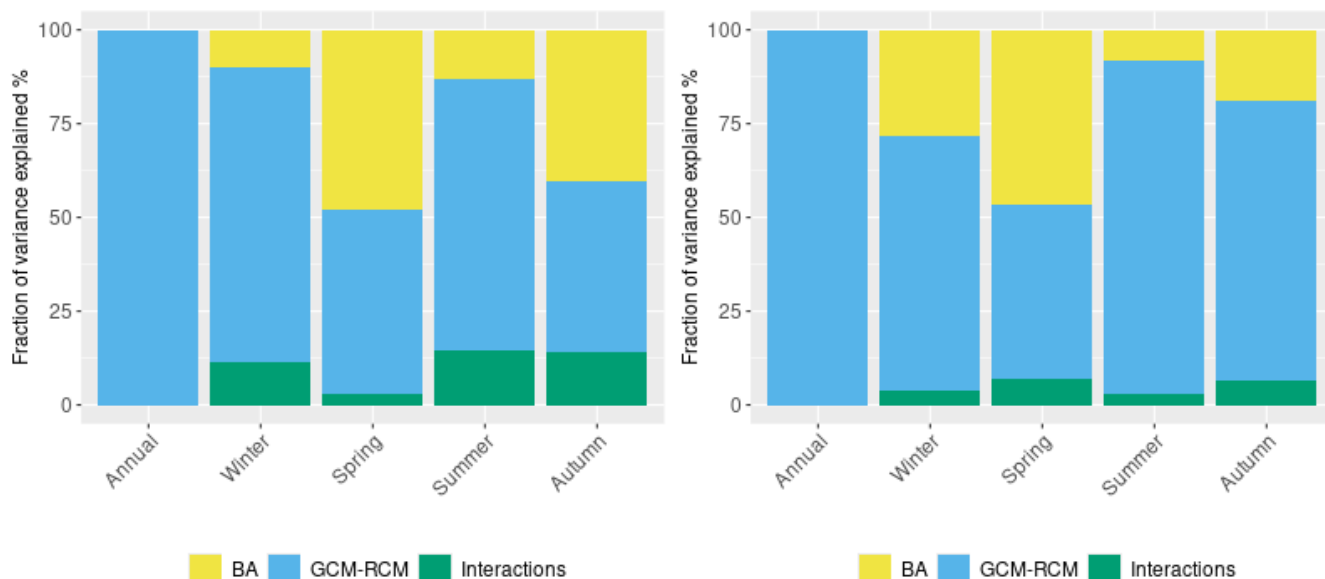
609 **7.3 Uncertainty analysis**

610 Besides the two different bias-adjustment methods, the various GCM-RCM combinations contribute to uncertainties in the
 611 climate projections. In this section, we analyse the contribution of these two uncertainty sources using the ANOVA method
 612 used by Vetter et al. (2017). Since each GCM is combined with different RCMs (see Section 4), we don't distinguish the
 613 GCMs and RCMs as different uncertainty sources here, but consider the GCM-RCM combinations as one uncertainty source.
 614 The two bias-adjustment methods are considered the second uncertainty source. The ANOVA method provides not only
 615 variations in the impact on temperature/precipitation from these two major sources, but also their interaction term. To avoid
 616 the bias caused by different sample sizes of the sources, the ANOVA was implemented for a number of subsamples, each of
 617 which includes two climate models and two bias correction methods, and then the obtained estimates of subsamples were
 618 averaged. For more explanation of the method and equations, please refer to Vetter et al. (2017).

619 Since our implementation of 3DBC conserves the annual changes from EQM, the annual fraction of variance from the ANOVA
 620 analysis (Fig. 14 and 15) is solely dependent on the GCM-RCM combination. On a seasonal scale, the largest contribution to
 621 temperature uncertainties still comes from the GCM-RCM combinations. However, for spring and autumn the bias-adjustment
 622 contribution can be of similar size, especially in the near future projections. Interactions between the two uncertainty sources
 623 are generally small.

624 For precipitation, the contribution to the overall uncertainty from the bias-adjustment methods is larger than the contribution
 625 from the climate models for spring and autumn in the near future. Also for the other two seasons, the different contributions
 626 are of similar size for the near future. Interestingly, for the far future, the contribution from the climate models is clearly larger

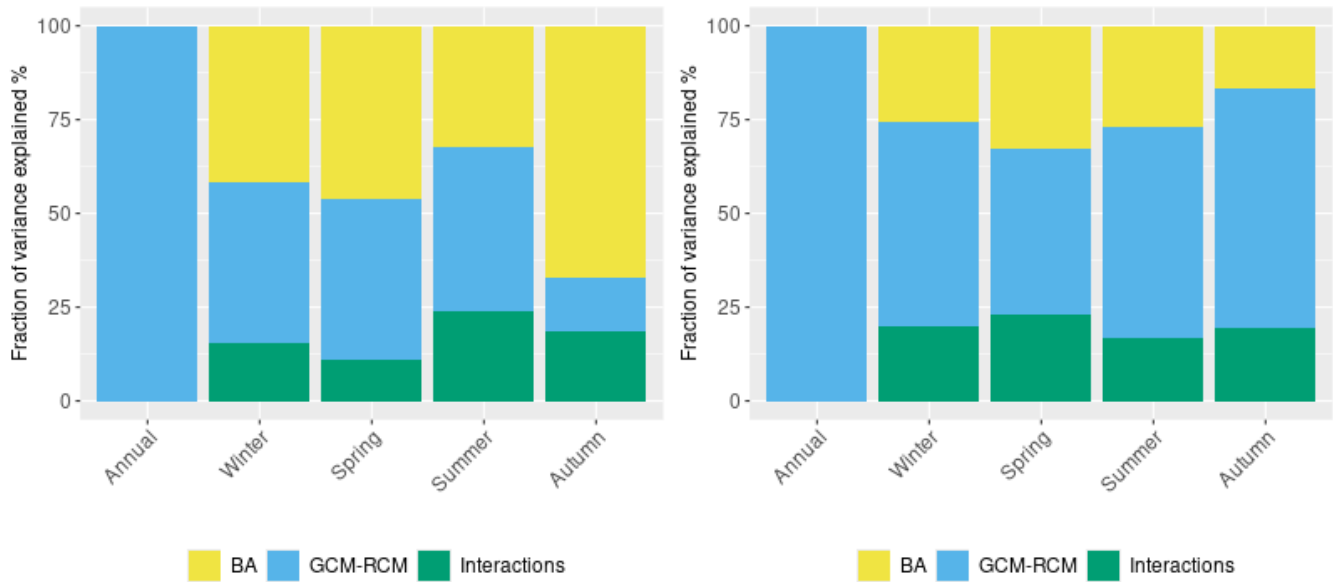
627 than the contribution from the bias-adjustment methods for all seasons. The interactions are larger than for temperature and
 628 can reach magnitudes similar to the single contributions. This is an effect of the two bias-adjustment methods resulting in
 629 seasonal change signals that differ more for precipitation than temperature, showing that results for temperature from a single
 630 bias-adjustment method are more robust than for precipitation. This is especially true for the near future.
 631



632

633 **Figure 14: the fraction of variance in projected temperature changes explained by bias-adjustment methods (BA), GCM-RCM**
 634 **combinations and their interactions for the near-future period (2041–2070, left) and far-future period (2071–2100, right).**

635



636

637

Figure 15: The same as Fig. 14 but for precipitation.

638

Our findings bring new insights into uncertainty attribution for seasonal projections, because most studies on uncertainty attribution are mainly targeted at annual values rather than seasonal ones, e.g. Paz and Willems (2022) and Lafferty and Sriver (2023). There are only a few uncertainty analyses for seasonal changes, but they did not find larger uncertainty associated with bias-adjustment methods than the variability within the model ensemble (Tong et al., 2021; Zhang et al., 2024). Our results highlight that bias-adjustment methods can be an important uncertainty source for seasonal projections and their seasonal effects should be considered in future studies.

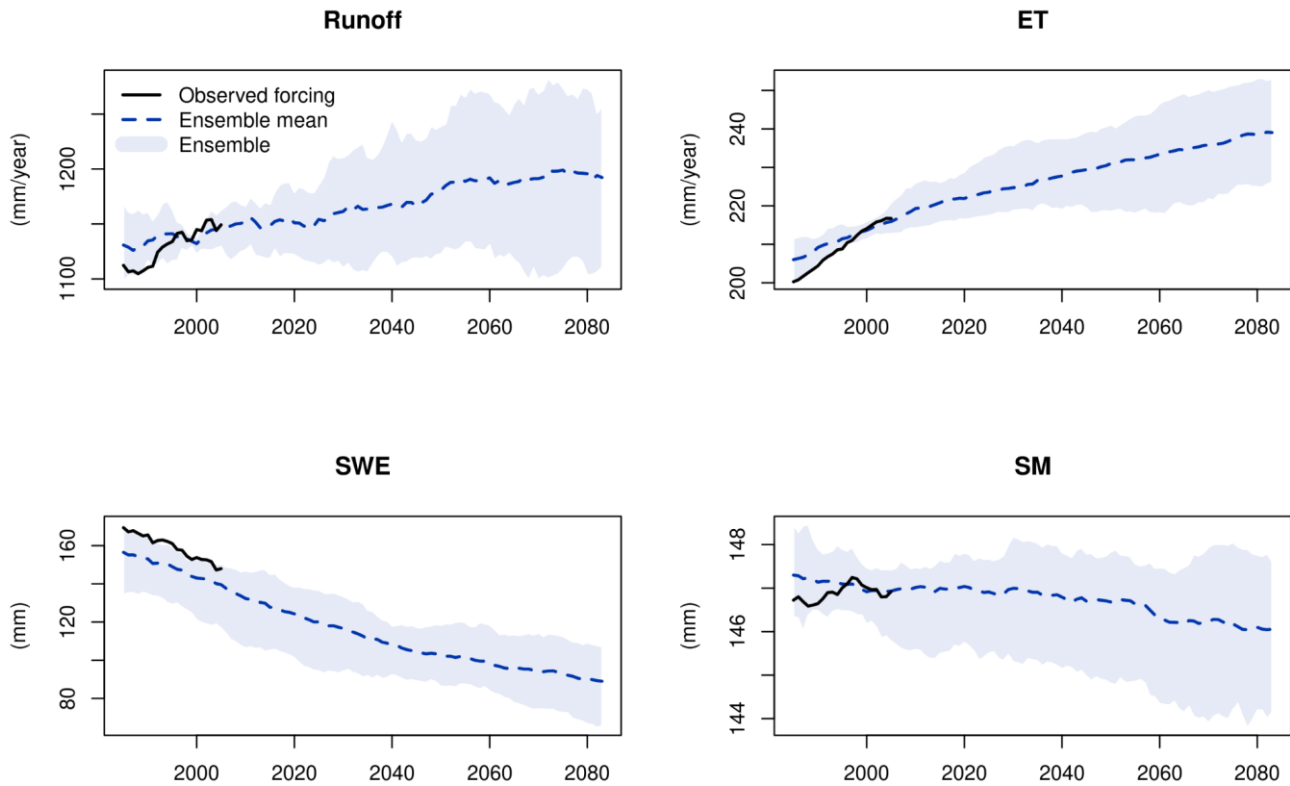
639

640

641

642

643



646

647 **Figure 16: Simulated 30-year running means of annual runoff, evaporation (ET), mean snow water equivalent (SWE) and mean soil**
 648 **moisture (SM) driven by the ensemble of 20 climate projections (10 GCM-RCMs x 2 bias correction methods) under the RCP4.5**
 649 **scenario. The black line is the simulated water components driven by the observed forcing data.**

650

651

652

653

654

655

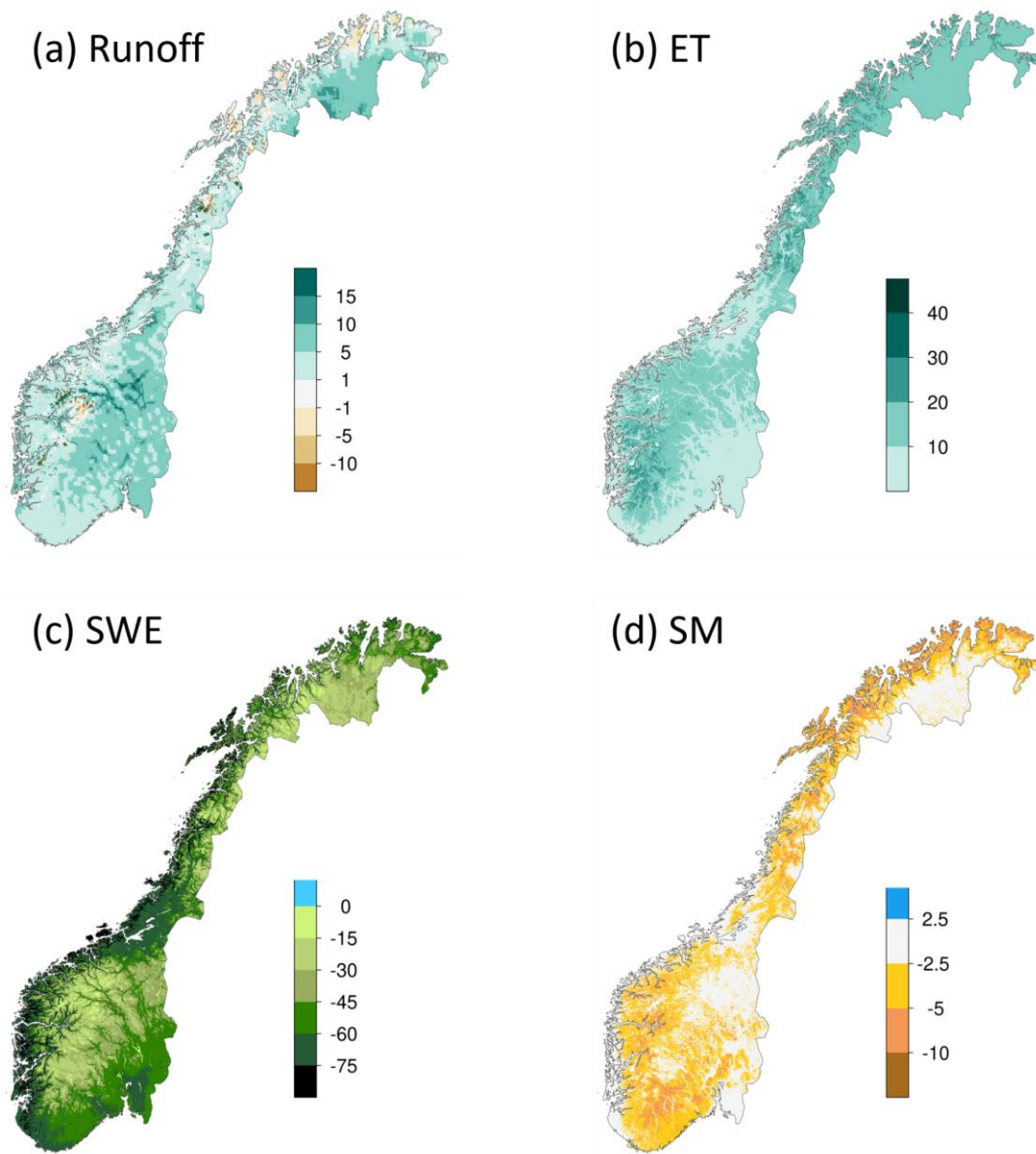
656

657

There are 20 hydrological projections for mainland Norway at 1km spatial resolution with daily time steps under the RCP4.5 scenario from the distHBV-COR-BA-2025 dataset. Figure 16 shows the projected annual sum/mean of these variables from 1971 to 2098 for mainland Norway. Both the ensemble means of runoff and evaporation have an increasing trend while the ensemble means of snow water equivalent and soil moisture trend to decrease towards the end of this century. The simulated runoff, evaporation, and soil moisture driven by the seNorge forcing data (black lines) are generally within the boundary of the 20 simulations in the historical period, and they have a good agreement with the ensemble mean around the year 2000. In addition, the spread of projections is reduced around the year 2000, as the bias-adjusted data matches the statistics of the observations better in the training period 1985-2014 than other periods. However, all snow water equivalent simulations are

658 generally underestimated compared with the simulated snow water equivalent driven by the seNorge data, indicating that snow
659 generation is not well reproduced. It is mainly due to inaccurate inter-variable, spatial and temporal dependence between the
660 bias-adjusted atmospheric variables when only the EQM method is used (see section 8.2).

661 Figure 17 shows the spatial distribution of the ensemble mean changes in the last scenario period (2071–2100) relative to the
662 reference period (1991–2020). In general, the increase in runoff is dominant in the whole country, except glacier retreat areas
663 around the glaciers and the coastal areas in the northern part of Norway. The increasing changes are minor (<5%) or moderate
664 (5–10%) in most parts of the country and strong increase in runoff (> 10%) occurs mainly in the glacier areas, lakes and rivers
665 as well as some northernmost areas. Due to the warmer and wetter climate in the future, evaporation is projected to increase
666 in the whole country, especially in western and central Norway. In contrast, the annual mean snow water equivalent will
667 decrease in the whole country in the far future, with a strong decrease (<-75%) along the coast. Note that snow volumes along
668 the coast of Southern Norway are small in today's climate. The absolute decrease in annual mean snow water equivalent is not
669 stronger along the coast than mountainous areas. Soil moisture will decrease in most parts of the country due to the increase
670 in evaporation and earlier snow melt, and moderate to strong decreases (<-5%) are mainly found in some southern areas and
671 the coastal regions in the north.

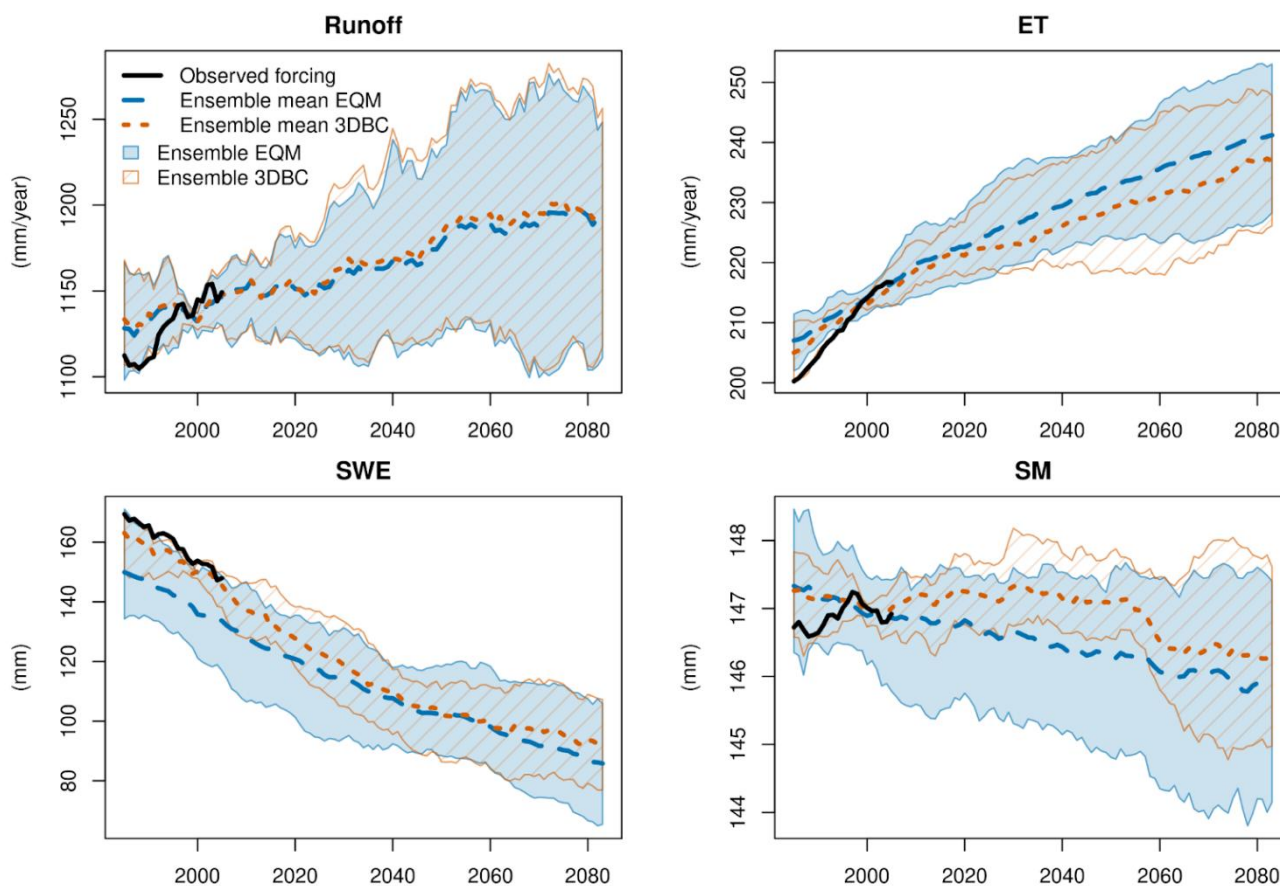


672
 673 **Figure 17: ensemble mean changes (%) in annual runoff (a), evaporation (ET) (b), snow water equivalent (SWE) (c) and soil moisture**
 674 **(SM) (d) in the scenario period 2071–2100 relative to the reference period 1991–2020 under the RCP4.5 scenario for mainland**
 675 **Norway.**

676 **8.2 Effects of the two bias-adjustment methods**

677 In this section, we provide a general overview of the effects of the bias-adjustment methods on hydrological projections. Figure
 678 18 shows again the projected annual sum/mean of hydrological variables from 1971 to 2098 for mainland Norway, but

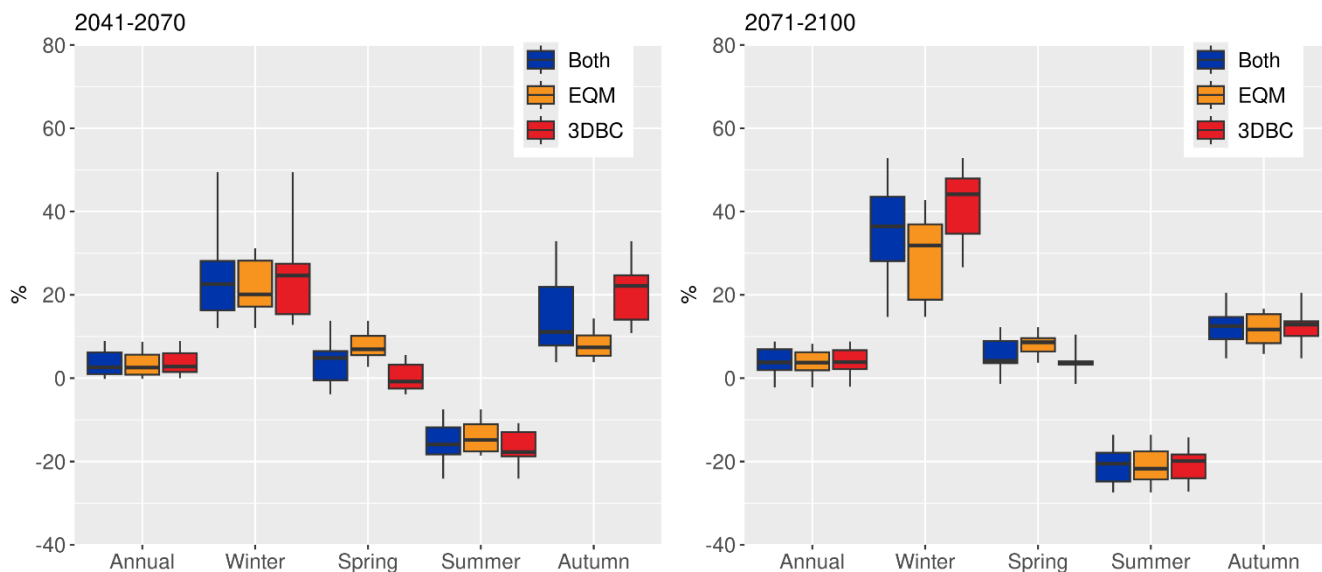
679 separating the projections between the two bias-adjustment methods. The results show that the two bias-adjustment methods
 680 play a minor role on ensemble means as well as ensemble spread for runoff, evaporation and soil moisture, with the differences
 681 between the bias-adjustment methods less than 10 mm/year for runoff and evaporation and less than 1 mm for soil moisture.
 682 The ensemble mean of snow water equivalent using the 3DBC method has a better agreement with the results driven by
 683 observed forcing data than the ensemble mean using the EQM method, which always leads to underestimation of snow water
 684 equivalent in the historical period. In addition, the ensemble spread for snow water equivalent is narrower using 3DBC than
 685 EQM, especially before 2040, indicating lower uncertainty of projections using 3DBC. However, it is interesting to see that
 686 the snow water equivalent projections do not differ substantially after 2040 between the two bias-adjustment methods, probably
 687 due to less snow days in a warming climate. The minor impact of bias-adjustment methods on annual values also leads to
 688 similar spatial distributions of the changes in runoff, evaporation and soil moisture, but considerable differences of changes in
 689 snow water equivalent are found along the coast and northmost Norway between the bias-adjustment methods (Fig. S3 in
 690 Supplementary material).



691

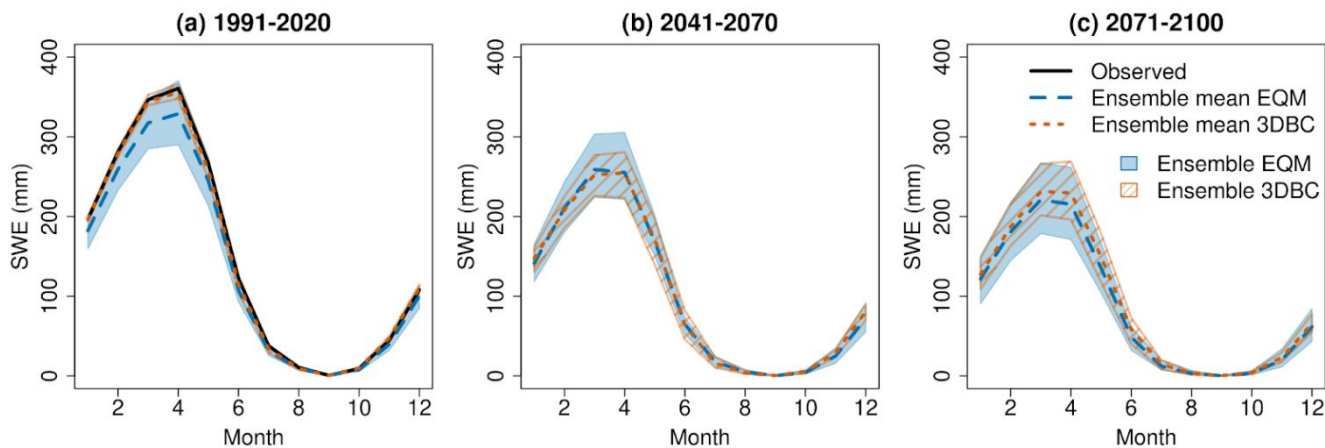
692 **Figure 18: The same as Fig. 16 but the projections using different bias-adjustment methods are separated.**

693 Although the bias-adjustment methods affect the annual changes in runoff marginally, they lead to different seasonal runoff
 694 changes and their effects vary in scenario periods and seasons. Figure 19 shows the seasonal relative changes in runoff
 695 including all 20 projections, 10 projections using the EQM bias-adjustment method and 10 projections using the 3DBC method,
 696 respectively. In the near future, the largest difference in the ensemble median changes between the bias-adjustment methods
 697 is found in autumn (ca. 13%), followed by the difference in spring (ca. 8%), winter (ca. 5%) and summer (ca. 3%). The 3DBC
 698 method leads to higher runoff changes in winter and autumn, but lower runoff changes in spring and summer than the EQM
 699 method. As a result, the two methods lead to similar changes in annual changes. In the far future, the bias-adjustment methods
 700 mainly affect the runoff changes in winter and spring, resulting in a difference in median changes of 12% in winter and 5% in
 701 spring. There is almost no difference in median runoff changes between the methods in summer and autumn. These results
 702 indicate that the two bias-adjusted methods mainly affect the snow accumulation and melt processes, which occur in autumn,
 703 winter and spring in the near future and in winter and spring in the far future. In addition, 3DBC always leads to higher runoff
 704 in winter and lower runoff in spring than EQM in both scenario periods.



705
 706 **Figure 19: relative changes in runoff for different seasons in the scenario periods 2041–2070 (left) and 2071–2100 (right) relative to**
 707 **the reference period 1991–2020 under the RCP4.5 scenario for mainland Norway.**

708
 709



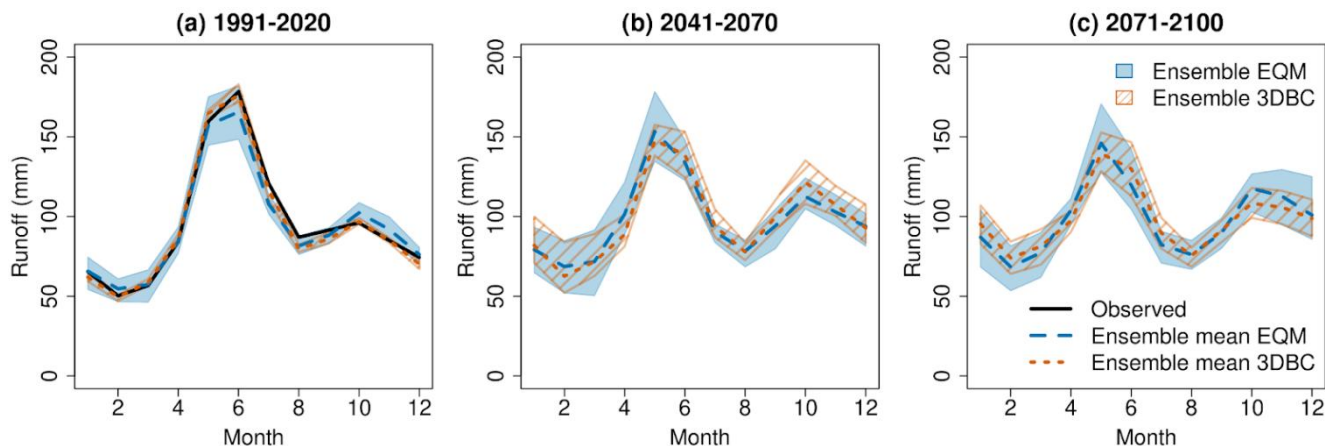
710

711 **Figure 20: Simulated monthly snow water equivalent (SWE) for mainland Norway using the EQM and 3DBC bias-adjusted climate**
 712 **projections.**

713 In order to illustrate the effects of the two bias-adjustment methods on snow processes, we compared the monthly snow water
 714 equivalent in the historical and scenario periods driven by different bias-adjusted projections as well as the ones driven by the
 715 observed forcing data (Fig. 20). In the historical period, the ensemble mean of monthly snow water equivalent driven by the
 716 3DBC bias-adjusted projections agrees well with the simulated one driven by the observed forcing data. The EQM bias-
 717 adjusted simulations generally lead to underestimation of monthly snow water equivalent, especially in March and April,
 718 similar to the findings by Meyer et al. (2019). In addition, the historical snow simulations using the EQM method vary
 719 substantially between climate models, while all bias-adjusted climate projections using the 3DBC method lead to similar
 720 monthly SWE, indicating more robust snow projections in the historical period using the 3DBC method than the EQM method.

721 The two bias-adjusted methods also affect the projected changes in snow water equivalent in the scenario periods, especially
 722 in the near future. The ensemble mean of monthly snow projections using the 3DBC methods show average decreases of about
 723 44 and 55 mm/month in the near and far future periods relative to the reference period respectively, while the ensemble mean
 724 using the EQM method decreases by 33 and 50 mm/month on average in the near and far future periods, respectively. It is due
 725 to higher snow water equivalent in the historical period and lower snow water equivalent in the near future using the 3DBC
 726 bias-adjusted projections than those using the EQM projections. However, the differences in snow water equivalent between
 727 the near and far-future periods are smaller using the 3DBC than the EQM method, leading to closer agreement on snow water
 728 equivalent changes in the far future between the two methods. The uncertainty bounds of snow projections using the 3DBC
 729 method are still smaller than the uncertainty bounds using the EQM method in both future periods, but the differences in
 730 uncertainty bounds between the two methods is less substantial than the ones in the historical period.

731



732

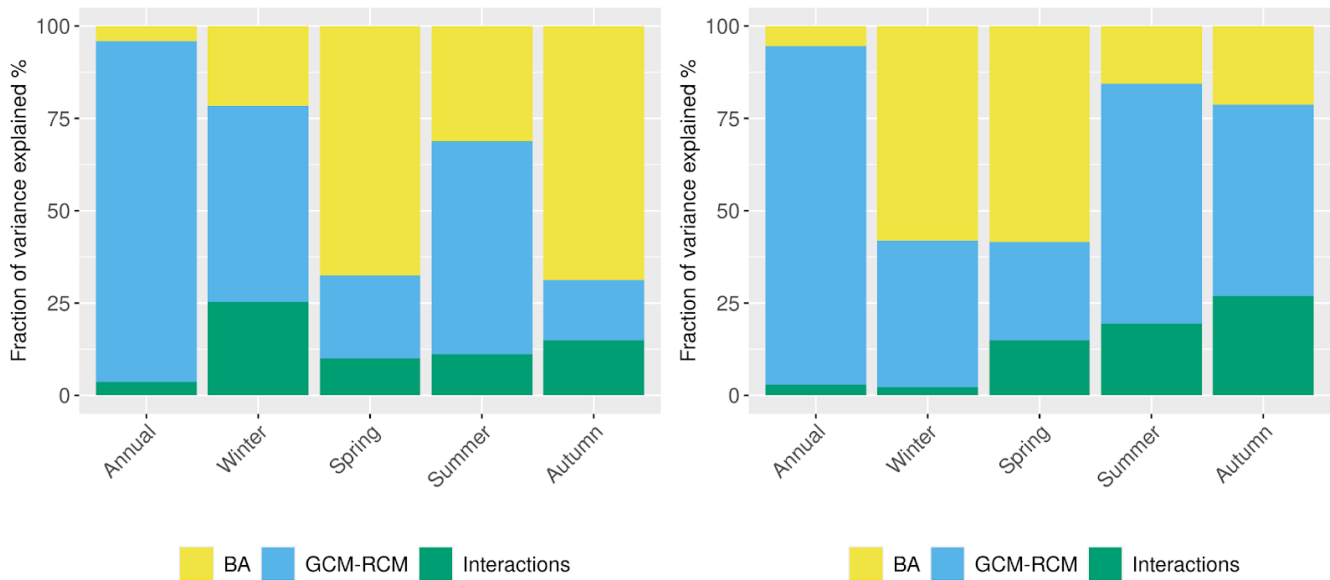
733 **Figure 21: The same as Fig. 20 but for runoff.**

734 Partly due to different snow simulations, the monthly runoff projections also differ between the two bias-adjustment methods
 735 (Fig. 21). In the historical period, the simulated runoff using the 3DBC bias-adjusted climate simulations also agrees well with
 736 the simulated runoff using observed forcing data, while the simulations using the EQM bias-adjusted climate simulations
 737 underestimate runoff from June to July that is generated by snow melt, mainly due to less snow storage in winter and spring
 738 (Fig. 20). There is also an overestimate of runoff from October to November using the EQM bias-adjusted climate simulations,
 739 indicating that other hydrological processes besides snow are also affected by the inaccurate spatial and temporal correlations
 740 of climate variables. Similarly, the runoff simulations using the EQM bias-adjusted climate projections have larger uncertainty
 741 bounds than the ones using the 3DBC projections.

742 In the future periods, the runoff projections using the 3DBC method show larger increase and decrease in monthly changes
 743 relative to the historical period than using the EQM ones. In addition, the 3DBC bias-adjusted climate projections lead to
 744 higher runoff in autumn in the near-future than in the far-future while the EQM projections show contradicting changes.
 745 Different from the snow projection uncertainty, the runoff uncertainty using the 3DBC method is not always smaller than the
 746 one using the EQM method in all months. In addition, the large runoff uncertainty in the historical and future periods does not
 747 lead to large uncertainty of runoff changes. As shown in Fig. 19, the uncertainty bounds of runoff changes using the 3DBC
 748 method is not substantially larger than the uncertainty of changes using the EQM method.

749 **8.3 Uncertainty analysis**

750



751

752 **Figure 22: the fraction of variance in runoff change projections explained by bias-adjustment methods (BA), GCM-RCM**
 753 **combinations and their interactions for the near-future period (2041-2070) (left) and far-future period (2071-2100).**

754 Similar to temperature and precipitation, we assessed the contribution of the two bias-adjustment methods and GCM-RCM
 755 combinations to the uncertainty in the runoff projections. Figure 22 shows the fraction of variance from the ANOVA analysis
 756 for the GCM-RCM combinations, bias-adjustment methods and their interactions for the two future periods. For both periods,
 757 it is obvious that the climate model combinations contribute to the majority of the annual runoff change variance (> 90%).
 758 However, the bias-adjustment methods play important roles in the seasonal runoff changes, especially in spring and autumn in
 759 the near future and in the winter and spring in the far future, explaining more than 50% of the runoff change variance. For
 760 summer, the climate model combinations are always the major uncertainty source, explaining more than 50% of the total runoff
 761 change variance. These results highlight the effects of bias-adjustment methods on seasonal runoff change projections.

762 9 Discussion

763 9.1 Limitations of the methodology

764 In this study, we present the whole modelling chain that produces the updated national ensembles of climate and hydrological
 765 projections for the new Climate in Norway report CiN-2025 (Dyrrdal et al., 2025). This modelling chain includes selection of
 766 emission scenarios and climate models, downscaling and bias-adjustment methods and hydrological models. Although we

767 have made a number of substantial improvements in each component of the modelling chain, there are still limitations and
768 weaknesses in the methodology, which require further development for future climate impact assessments.

769 The first component in the modelling chain is to select appropriate emission scenarios and climate projections from a large
770 ensemble of GCM and RCM outputs manageable throughout the complete chain. As a national climate assessment report
771 following the sixth IPCC report, it would have been ideal to apply the most updated emission scenarios (i.e., the SSPs) and the
772 corresponding climate projections. However, due to the long time needed to make the newest RCM results available within
773 the CORDEX framework and the time limit of the national report, we had to apply the climate projections corresponding to
774 the fifth IPCC report for the low- and median emission scenarios (RCP scenarios). Complements of the national climate
775 projections for SSP emission scenarios are expected in the future to provide up-to-date knowledge on climate change impacts.

776 Since the EURO-CORDEX ensemble for the RCP scenarios is now much larger than for CiN-2015, the climate projections
777 for CiN-2025 are more representative of the full range of climate changes ensembles. However, the restriction to ten models
778 per scenario stemming from the complete modelling chain still partly limits the representativeness of the full possible outcome
779 and model variability. In CiN-2025, this limitation is taken into account for temperature and precipitation using results from
780 empirical-statistical downscaling (ESD) of the complete set of available GCMs. The ESD results are shown in the CiN-2025
781 report but not in this study as our focus is on the complete modelling chain. A detailed description of the ESD method used in
782 CiN-2025 is given in Benestad et al. (2025).

783 RCMs are still subject to general limitations of model simplifications, such as internal parameterizations and spatial resolution.
784 Further, some technical limitations remain in the RCM outputs, for example, some models provide outputs for 360 days per
785 year, no leap year days or start in 1970 and end in 2098. This brings challenges for impact models and requires pre-processing
786 before bias-adjustment. In addition, the historical period simulated by the RCMs does not cover the current standard normal
787 period (1991–2020). This is a drawback since it is easier for the general public to compare the climate change signals with
788 respect to the climate normal than other non-standard periods (e.g., 1976–2005). Although the use of the first few years from
789 the scenario projections as reference period is not optimal, and the choice of the reference period can lead to different climate
790 changes signals (Liersch et al., 2020), the use of the most recent standard normal period improves the public acceptance and
791 understandability substantially, which is most important for the target users of a national report such as CiN-2025.

792 As the second component of the modelling chain, downscaling and bias-adjustment methods allow presenting projected climate
793 and hydrological changes at a spatial resolution of 1x1 km for the complex topography of Norway. Providing such high
794 resolution data needs high computational costs and makes it challenging to test and apply a large number of bias-adjustment
795 methods. Hence, we only selected EQM as the bias-adjustment method as it is robust for different climatological regimes and
796 well established. The 3DBC method is further applied on the EQM bias-adjusted variables to improve the inter-variable, spatial
797 and temporal dependencies. This multivariate bias-adjustment method indeed improves the hydrological projections,

798 especially for snow simulations, and reduces the uncertainty range, especially in the reference period. However, the 3DBC
799 method (Section 5.3) leads to different climate change signals compared to the original RCM signals on sub-annual scales
800 because it imposes temporal dependency structures on the future projections similar to the ones from the reference datasets.
801 This may be considered a weakness of the approach and more evaluation and development of multivariate bias-adjustment
802 methods are required to further improve the existing methods. As discussed in François et al. (2020), the choice of method
803 may differ from case to case, depending on which statistical properties from the RCMs need to be preserved or corrected.
804 Based on our findings, users of the bias-adjusted data may select the appropriate dataset depending on their needs, or simply
805 consider the two methods being equal, resulting in a broader ensemble.

806 In this study, RCM outputs have firstly been interpolated to the resolution of the observations (1 km) using the nearest-
807 neighbour method and then bias-adjusted on that resolution. However, users should not overinterpret projected changes which
808 are finer than the native RCM resolution (~12.5 km) as the resolving power of the RCM sets the natural lower limit on which
809 local-scale physical processes can be considered. Maraun (2013) has shown that the quantile mapping method cannot resolve
810 this scale mismatch. This effect might be less important for temperature than precipitation as temperature usually has a much
811 higher spatial coherence while precipitation is more subjected to small-scale variability. Although generally both the EQM
812 and the 3DBC methods in our setup do not bring in climate change signals below the RCM resolution, some artifacts might be
813 introduced which do not represent true local, small-scale climate changes.

814 Regarding hydrological models, both the potential evaporation module and glacier modelling have been improved compared
815 to the model used in CiN-2015. The Penman-Monteith method improves evaporation estimates under climate scenarios by
816 considering more climate variables and representing different land cover types (Huang et al., 2026), while the dynamic glacier
817 modelling by DEW successfully avoids unrealistically high runoff from the glacier retreat areas under a warming climate.
818 However, the simulations of distHBV may still suffer equifinality problems due to a large number of calibration parameters,
819 which do not represent the physical characteristics of specific land use and soil types. In addition, we reclassify the soil types
820 into five major groups in order to reduce the number of calibration parameters related to soil processes. This may lead to
821 unreliable simulations for the areas where the soil condition is largely different from the major soil types. Therefore, both the
822 calibration procedure and the spatial representation of soil physical characteristics are expected to improve in the future
823 national applications.

824 Last but not least, vegetation types and characteristics are static in our hydrological modelling under climate change scenarios,
825 but the changes in vegetation characteristics are expected under a warming climate. Huang et al. (2025a) assessed the effects
826 of forest growth and forest management on water resources in six Norwegian catchments under the RCP2.6 and RCP4.5
827 emission scenarios. They found that forest growth would offset the increase in runoff in the catchments, where the deciduous
828 forest is dominant. It implies that the runoff in the deciduous forest areas, especially in North Norway, may be overestimated

829 in our present runoff projections. For the next generation CiN report, the land use and vegetation change scenarios should be
830 included in the hydrological modelling if such scenarios are available.

831 **9.2 Comparison of results between the old and new national reports**

832 The improved modelling chain generated updated climate and hydrological projections for Norway, which resulted in slightly
833 different climate change signals and climate impacts compared to the analysis in the old national report. Under the RCP4.5
834 scenario, the projections for the old and new national reports agree on the direction of change, but CiN-2025 projections display
835 a smaller increase in annual temperature (ensemble mean of 2.0 °C) and precipitation (ensemble mean of 6%) than the
836 ensemble means in CiN-2015 (2.7 °C and 8% increase in temperature and precipitation respectively) at the end of the century.
837 In addition, the ensemble spread in CiN-2025 is narrower than in CiN-2015, indicating more robust climate change signals.
838 However, these differences are caused not only by the new selection of climate models, but also by the selection of the reference
839 period. In CiN-2015, 1971–2000 was used as the reference period while in CiN-2025, it is 1991–2020. As temperature has
840 already risen considerably in recent decades in Norway, annual mean temperature is higher in 1991–2020 than in 1971–2000,
841 and the differences in temperature between the periods 2071–2100 and 1991–2020 are consequently more moderate than those
842 between 2071–2100 and 1971–2000. In contrast, a larger increase in runoff is seen in CiN-2025 projections than in the previous
843 one, mainly due to the improved evapotranspiration routine in the hydrological model (Huang et al., 2026).

844 Another major difference between the old and new national report is that CiN-2025 selected SSP3-7.0 as the high-emission
845 scenario, which assumes lower emission than RCP8.5 used in CiN-2015. Under SSP3-7.0, the ensemble mean increases in
846 annual mean temperature, precipitation and runoff are 3.4 °C, 11% and 10% in 2071-2100 relative to 1991-2020, respectively
847 (Fig. S4, S5 and S16 in Supplementary materials). These increases are also smaller than the ones in 2071-2100 relative to
848 1971-2000 under the RCP8.5 scenario, shown in the old national report. Hence, users who have made computations based on
849 the CiN-2015 projections, should notice these differences and justify whether their computations should be updated or not.

850 **9.3 The effects of bias-adjustment methods under the high-emission scenario SSP3-7.0**

851 This paper comprehensively compared the two bias-adjustment methods applied to EURO-CORDEX RCP4.5 simulations and
852 found that the two methods can lead to considerable differences in seasonal changes and snow simulations under the moderate-
853 emission scenario. However, the impact of the bias-adjustment methods may not only vary between climate models and future
854 periods but also between emission scenarios. Thus, results for the same comparison between the two bias-adjustment methods
855 under SSP3-7.0 are included in the Supplementary material (Figures S6-S19). Although the magnitudes of the projected
856 changes between SSP3-7.0 and RCP4.5 differ, the general effects and differences between the two bias-adjustment methods

857 are similar. One interesting aspect is a generally better agreement of the SSP3-7.0 ensemble mean temperature and precipitation
858 with the observed values than in the RCP4.5 simulations during the reference period (Fig. S4).

859 For hydrological projections, 3DBC still provides better historical simulations than EQM under the SSP3-7.0 scenario, but the
860 difference in future projections varies between the bias-adjustment methods and seasons. Considerable differences of ensemble
861 mean changes in runoff are found in all seasons in the near future and in winter in the far future. The ensemble spreads of
862 monthly projections for snow water equivalent and runoff are similar between 3DBC and EQM for almost all months,
863 indicating that 3DBC does not help to reduce the projection uncertainty substantially under extremely warm conditions.

864 **9.4 Application**

865 Despite the limitations mentioned above, the COR-BA-2025 and distHBV-COR-BA-2025 datasets generated by the presented
866 modelling chain provide the most updated, comprehensive and detailed hydrometeorological projections for mainland Norway.
867 These national projections serve as the scientific basis for research on climate change impacts in Norway. The gridded
868 hydrometeorological projections from CiN-2015 have already been used to derive new indices for specific application, e.g.
869 snow-dependent tourism (Kuya et al., 2024; Mayer et al., 2023), reindeer husbandry (Hanssen-Bauer et al., 2022), frost decay
870 exposure on building projects (Gaarder et al., 2024) and road maintenance (Nilsen et al., 2021). In addition to impact modellers,
871 who represent an advanced user group, NCCS aims at providing tailored information for practical climate adaptation. Products
872 derived from the national projections have also been widely used in local planning, mainly because government guidelines
873 (Norwegian Government, 2024) required municipalities to take climate change into account in planning. Climate factsheets
874 (Hisdal et al., 2021) provided the most relevant information to guide the climate adaptation work, and were pointed out as a
875 core reference in government guidelines. See Nilsen et al. (2022) for an overview of the steps from climate model output to
876 actionable climate information.

877 Besides the possibility to update existing applications that used the gridded dataset from CiN-2015, the new COR-BA-2025
878 and distHBV-COR-BA-2025 datasets provide additional variables, such as wind speed, pressure, evaporation, radiation and
879 relative humidity, each bias-adjusted both with EQM and 3DBC. This improves the utility of the dataset for e.g., ecological
880 modelling (see Pirk et al., 2023 for an example). It is expected that the new dataset will facilitate use in an even wider range
881 of applications in the coming years, for climate change impacts on e.g., glaciers, drought, landslides and water availability.
882 Further work will involve user groups such as municipal planners to co-create climate services based on the
883 hydrometeorological projections presented.

884 In principle, we suggest using the full ensemble projections with both bias-adjustment methods to account for the uncertainty
885 of the whole modelling chain. But in practice, users may want to select a subset of climate models and one bias-adjustment
886 method to reduce the computational cost of further applications. As the users may be only interested in parts of Norway and

887 the performance of climate models and bias-adjustment methods vary in space and time, we are not able to give a
888 straightforward suggestion on the subset of climate models and bias-adjustment methods based on the national analysis.
889 However, the methodology as well as the analysis in this paper provides examples of selecting models and bias-adjustment
890 methods. In order to select a subset of climate models, the users can analyze the climate signals for their study area and periods
891 as in Fig. 3 and then select the models based on the study purpose, e.g., studies aiming to assess the driest and warmest climate
892 conditions or the wettest and coldest conditions in the near or far future. Based on the selected models, the users can further
893 assess the seasonal trends for their study area and periods using both EQM and 3DBC projections as in Fig. 6. If the trends are
894 comparable between the two bias-adjustment methods, the 3DBC adjusted projections can be preferred, especially when the
895 study is focused on seasonal changes and snow processes. Otherwise, we strongly recommend to use the projections adjusted
896 by EQM and 3DBC to account for the uncertainty of bias-adjustment methods.

897 Finally, we should note that the gridded datasets distHBV-COR-BA-2025 are not designed to use for flood indices, or climate
898 change allowances for floods because distHBV was calibrated against many catchments simultaneously. Instead, the outputs
899 from specific flood models should be used (Lawrence, 2020; Carr et al., 2023). The flood models include two lumped
900 hydrological models and were calibrated against observed discharges for each catchment separately. Hence, the flood models
901 produce more reliable estimates of high (and low) flow for specific catchments.

902 **10 Conclusions**

903 In this study, we present the whole modelling chain behind the production of updated national ensembles of climate and
904 hydrological projections for the official “Climate in Norway” assessment report. We also provide insight into the
905 hydrometeorological projections, which we termed COR-BA-2025 (standing for CORDEX-Bias Adjusted, updated in 2025)
906 for climate projections and distHBV-COR-BA-2025 for hydrological projections, and analyse their uncertainties. The
907 modelling chain (Fig. 2) includes the selection of GCM-RCM combinations for Norway from a large ensemble of EURO-
908 CORDEX simulations, the application of two bias-adjustment methods and distributed hydrological modelling including a
909 physically-based potential evaporation approach and a dynamic glacier model. Compared to the previous national assessment
910 report, the new climate projections are considered more representative for Norway due to a larger ensemble of EURO-
911 CORDEX simulations taken into account and a systematic analysis of the projections.

912 A multivariate bias-adjustment method has been applied for the first time over the whole of Norway for the complete
913 atmospheric dataset consisting of nine variables. This new method leads to more consistent data in space, time and between
914 variables, and to more robust hydrological simulations than the univariate empirical quantile mapping method (especially for
915 snow and in the reference period), but it does not preserve climate change signals on a sub-annual scale. However, the
916 uncertainty ranges of runoff change projections are not significantly different between the two bias-adjustment methods,

917 especially at the annual scale. An uncertainty analysis shows that the climate projections are the major source of uncertainty
918 for annual runoff change, while the selection of the bias-adjustment method plays an important role on seasonal changes.

919 Despite the advancement in the presented methodologies and modelling chain, there is still room for further improvement in
920 future climate impact assessment studies. Currently we foresee that additional emission scenarios and GCM-RCM
921 combinations from the EURO-CORDEX initiative will be evaluated and the bias-adjustment methods will be further developed
922 to overcome the current limitations. In addition, the calibration procedure and the calibration parameters in the hydrological
923 modelling will be further improved using advanced machine learning techniques. If possible, the land use and vegetation
924 changes scenarios should also be considered in hydrological modelling.

925 The methodological description provided here serves as core knowledge for any further application of the gridded products,
926 which are expected to be used in a wide range of climate impact assessments and development of climate adaptation strategies
927 in Norway. We have thrived to meet the FAIR principles (Wilkinson et al., 2016) for data management. Thus, the complete
928 COR-BA-2025 and distHBV-COR-BA-2025 datasets (Wong et al. 2025) are findable and accessible through the Arctic Data
929 Centre (adc.met.no) at <https://doi.org/10.21343/0k90-6w67>. The data is stored in NetCDF format following the attribute
930 convention for data discovery (ACDD version 1-3, https://wiki.esipfed.org/Attribute_Convention_for_Data_Discovery_1-3)
931 and the climate and forecast metadata conventions (CF version 1.10, Eaton et al., 2022). The code and data are reusable, being
932 open source with non-restrictive licenses.

933 **Code availability**

934 The code of distHBV is available at <https://doi.org/10.5281/zenodo.17531118> (Beldring, 2025a)

935 The code of DEW is available at <https://doi.org/10.5281/zenodo.17530242>, (Beldring, 2025b)

936 The R source code of the 3DBC implementation used in this work is available at <https://doi.org/10.5281/zenodo.15260334>
937 (Dobler, 2025).

938 EQM implementation used the functions *fitQmapQUANT* and *doQmapQUANT* from R package *qmap* which is available at
939 <https://doi.org/10.32614/CRAN.package.qmap> (Gudmundsson, 2025).

940 **Data availability**

941 The **COR-BA-2025** and **distHBV-COR-BA-2025** bias-adjusted daily high-resolution climate and hydrological projections
942 for Norway are freely available at the Arctic Data Centre (adc.met.no) under <https://doi.org/10.21343/0k90-6w67> (Wong et
943 al., 2025).

944 The reference datasets used in the modelling chain are available at <https://doi.org/10.21343/gbq0-4t97> (Huang et al., 2025b).

945 **Author contribution**

946 SM, SLS, TL, WKW and AD performed the analysis of climate model selections and collected the RCM data. WKW and AD
947 designed the bias-adjustment experiments and methods and carried them out. IH modified the model code distHBV and IH
948 and SH performed the simulations. SB and KM developed the model code DEW, designed the experiments of DEW and GR
949 performed the simulations. SH prepared the manuscript with contributions from all co-authors. AVD, HOH, IBN and SJB
950 coordinated the whole project.

951 **Competing interests**

952 The authors declare that they have no conflict of interest.

953 **Acknowledgement**

954 We acknowledge the World Climate Research Programme, the CORDEX Science Advisory Team (SAT) - coordinating body
955 of CORDEX, and the Working Group on Coupled Modelling (WGCM) - responsible panel for CMIP5 and CMIP6. We thank
956 the CORDEX climate modeling groups (listed in Table 1 and S1) for producing and making available their model output,
957 CMIP5 and CMIP6 for providing the driving data, the Earth System Grid Federation (ESGF) for providing access, and the
958 multiple funding agencies who support CORDEX, CMIP and ESGF.

959 **Financial support**

960 This article was funded by the Norwegian Centre for Climate Services, and thus supported by the Norwegian Environment
961 Agency and the Ministry of Climate and Environment in addition to in-kind contributions from the Norwegian Water
962 Resources and Energy Directorate, NORCE and the Norwegian Meteorological Institute.

963 **References**

964 Ahlstrøm, A., Bjørkelo, K., and Frydenlund, J.: AR5 klassifikasjonssystem - klassifikasjon av arealressurser, Skog og
965 landskap, rapport nr. 6/2014, 38 pp. <http://hdl.handle.net/11250/2440173>, 2014.

966 Alifu, H., Hirabayashi, Y., Imada, Y., and Shioyama, H.: Enhancement of river flooding due to global warming, Sci Rep, 12,
967 20687, <https://doi.org/10.1038/s41598-022-25182-6>, 2022.

968 Andreassen, L. M., Huss, M., Melvold, K., Elvehøy, H. og Winsvold, S. H.: Ice thickness measurements and volume
969 estimates for glaciers in Norway. *Journal of Glaciology*, 61(228), 763-775. <https://doi.org/10.3189/2015JoG14J161>, 2015.

970 Astagneau, P. C., Wood, R. R., Vrac, M., Kotlarski, S., Vaittinada Ayar, P., François, B., and Brunner, M. I.: Impact of bias
971 adjustment strategy on ensemble projections of hydrological extremes. *Hydrol. Earth Syst. Sci.*, 29, 5695–5718,
972 <https://doi.org/10.5194/hess-29-5695-2025>, 2025.

973 Beck, H. E., Zimmermann, N. E., McVicar, T. R., Vergopolan, N., Berg, A., and Wood, E. F.: Present and future Köppen-
974 Geiger climate classification maps at 1-km resolution, *Sci Data*, 5, 180214, <https://doi.org/10.1038/sdata.2018.214>, 2018.

975 Beldring, S.: Distributed element water balance model system. *Norwegian Water Resources and Energy Directorate, Report*
976 *no. 4/2008*, 40 pp. https://publikasjoner.nve.no/report/2008/report2008_04.pdf
977 https://github.com/DistributedElementWaterModel/Version_3.03, 2008.

978 Beldring, S.: nve-sbe/DistributedHbv: v_1 (v_1), Zenodo, <https://doi.org/10.5281/zenodo.17531118>, 2025a.

979 Beldring, S.: DistributedElementWaterModel/Version_3.03: v_1 (v_1), Zenodo, <https://doi.org/10.5281/zenodo.17530242>,
980 2025b.

981 Beldring, S., Engeland, K., Roald, L. A., Sælthun, N. R., and Voksø, A.: Estimation of parameters in a distributed precipitation-
982 runoff model for Norway, *Hydrology and Earth System Sciences*, 7, 304–316, <https://doi.org/10.5194/hess-7-304-2003>, 2003.

983 Benestad, R. E., Parding, K. M., and Dobler, A.: Downscaling the probability of heavy rainfall over the Nordic countries,
984 *Hydrol. Earth Syst. Sci.*, 29, 45–65, <https://doi.org/10.5194/hess-29-45-2025>, 2025.

985 Bremnes, J. B.: Probabilistic wind power forecasts using local quantile regression, *Wind Energy*, 7, 47–54,
986 <https://doi.org/10.1002/we.107>, 2004.

987 Bright, R. M., Eisner, S., Lund, M. T., Majasalmi, T., Myhre, G., and Astrup, R.: Inferring Surface Albedo Prediction Error
988 Linked to Forest Structure at High Latitudes, *Journal of Geophysical Research: Atmospheres*, 123, 4910–4925,
989 <https://doi.org/10.1029/2018JD028293>, 2018.

990 Bürger, G., Sobie, S. R., Cannon, A. J., Werner, A. T., and Murdock, T. Q.: Downscaling Extremes: An Intercomparison of
991 Multiple Methods for Future Climate, *Journal of Climate*, 26, 3429–3449, <https://doi.org/10.1175/JCLI-D-12-00249.1>, 2013.

992 Carr, S., Lawrence, D., Skaugen, T., and Wong, W. K.: Projected future changes in peak flows and implications for climate
993 change allowances, NVE report nr. 26/2023, The Norwegian Water Resources and Energy Directorate, Oslo, Norway,
994 https://publikasjoner.nve.no/rapport/2023/rapport2023_26.pdf, 2023.

995 Cannon, A.J., Sobie, S.R. and Murdock, T.Q.: Bias Correction of GCM Precipitation by Quantile Mapping: How Well Do
996 Methods Preserve Changes in Quantiles and Extremes? *Journal of Climate*, 28, 6938-6959, [https://doi.org/10.1175/JCLI-D-](https://doi.org/10.1175/JCLI-D-14-00754.1)
997 [14-00754.1](https://doi.org/10.1175/JCLI-D-14-00754.1), 2015.

998 CH2018: CH2018 – Climate Scenarios for Switzerland, Technical Report. National Centre for Climate Services, Zürich, 271
999 pp, ISBN: 978-3-9525031-4-0, 2018.

1000 Chinita, M. J., Richardson, M., Teixeira, J., and Miranda, P. M. A.: Global mean frequency increases of daily and sub-daily
1001 heavy precipitation in ERA5, *Environ. Res. Lett.*, 16, 074035, <https://doi.org/10.1088/1748-9326/ac0caa>, 2021.

1002 Dalelane, C., Früh, B., Steger, C., and Walter, A.: A Pragmatic Approach to Build a Reduced Regional Climate Projection
1003 Ensemble for Germany Using the EURO-CORDEX 8.5 Ensemble, <https://doi.org/10.1175/JAMC-D-17-0141.1>, 2018.

1004 DCCEEW: National Climate Risk Assessment: Methodology. Department of Climate Change, Energy, the Environment and
1005 Water, <https://www.dcceew.gov.au/climate-change/publications/national-climate-risk-assessment>, 2023.

1006 Dobler, A.: doblone/3DBC: Version 2023 (Versjon v2023), Zenodo, <https://doi.org/10.5281/zenodo.15260335>, 2025.

1007 Dobrowski, S. Z., Abatzoglou, J. T., Greenberg, J. A., and Schladow, S. G.: How much influence does landscape-scale
1008 physiography have on air temperature in a mountain environment?, *Agricultural and Forest Meteorology*, 149, 1751–1758,
1009 <https://doi.org/10.1016/j.agrformet.2009.06.006>, 2009.

1010 Doherty, J. and Skahill, B. E.: An advanced regularization methodology for use in watershed model calibration, *Journal of*
1011 *Hydrology*, 327, 564–577, <https://doi.org/10.1016/j.jhydrol.2005.11.058>, 2006.

1012 Dunn, R. J. H., Alexander, L. V., Donat, M. G., Zhang, X., Bador, M., Herold, N., Lippmann, T., Allan, R., Aguilar, E., Barry,
1013 A. A., Brunet, M., Caesar, J., Chagnaud, G., Cheng, V., Cinco, T., Durre, I., de Guzman, R., Htay, T. M., Wan Ibadullah, W.
1014 M., Bin Ibrahim, M. K. I., Khoshkam, M., Kruger, A., Kubota, H., Leng, T. W., Lim, G., Li-Sha, L., Marengo, J., Mbatha, S.,
1015 McGree, S., Menne, M., de los Milagros Skansi, M., Ngwenya, S., Nkrumah, F., Oonariya, C., Pabon-Caicedo, J. D., Panthou,
1016 G., Pham, C., Rahimzadeh, F., Ramos, A., Salgado, E., Salinger, J., Sané, Y., Sopaheluwakan, A., Srivastava, A., Sun, Y.,
1017 Timbal, B., Trachow, N., Trewin, B., van der Schrier, G., Vazquez-Aguirre, J., Vasquez, R., Villarroel, C., Vincent, L., Vischel,
1018 T., Vose, R., and Bin Hj Yussof, M. N.: Development of an Updated Global Land In Situ-Based Data Set of Temperature and
1019 Precipitation Extremes: HadEX3, *Journal of Geophysical Research: Atmospheres*, 125, e2019JD032263,
1020 <https://doi.org/10.1029/2019JD032263>, 2020.

1021 Dyrrdal, A.V., Bakke, S.J., Hanssen-Bauer, I., Mayer, S., Nilsen, I.B., Nilsen, J.E.Ø., Paasche, Ø., Saloranta, T., Årthun, M.
1022 [editors]: Klima i Norge – kunnskapsgrunnlag for klimatilpasning oppdatert i 2025 (“Climate in Norway – knowledge base
1023 for climate adaptation updated in 2025”), NCCS Report 1/2025, Norwegian Centre for Climate Services, Oslo, Norway. (In
1024 Norwegian.). <https://doi.org/10.60839/4rgq-nn84>, 2025.

1025 Eaton, B., Gregory, J., Drach, B., Taylor, K., Hankin, S., Caron, J., Signell, R., Bentley, P., Rappa, G., Höck, H., Pamment,
1026 A., Jukes, M., Raspaud, M., Blower, J., Horne, R., Whiteaker, T., Blodgett, D., Zender, C., Lee, D., Hassell, D., Snow, A. D.,
1027 Kölling, T., Allured, D., Jelenak, A. Soerensen, A. M., Gaultier, L., Herlédan, S.: NetCDF Climate and Forecast (CF) Metadata
1028 Conventions (1.10). CF Community. <https://doi.org/10.5281/zenodo.14275561>, 2022.

1029 EEA (European Environment Agency): Energy Performance of Buildings Directive.
1030 <https://energy.ec.europa.eu/topics/energy-efficiency/energy-performance-buildings/energy-performance-buildings->
1031 [directive_en](https://energy.ec.europa.eu/topics/energy-efficiency/energy-performance-buildings/energy-performance-buildings-), last access: 19 August 2025.

1032 Erlandsen, H. B., Beldring, S., Eisner, S., Hisdal, H., Huang, S., and Tallaksen, L. M.: Constraining the HBV model for robust
1033 water balance assessments in a cold climate, *Hydrology Research*, 52, 356–372, <https://doi.org/10.2166/nh.2021.132>, 2021.

1034 Eum, H.-I., Gupta, A., and Dibike, Y.: Effects of univariate and multivariate statistical downscaling methods on climatic and
1035 hydrologic indicators for Alberta, Canada, *Journal of Hydrology*, 588, 125065, <https://doi.org/10.1016/j.jhydrol.2020.125065>,
1036 2020.

1037 Eyring, V., Bony, S., Meehl, G. A., Senior, C. A., Stevens, B., Stouffer, R. J., and Taylor, K. E.: Overview of the Coupled
1038 Model Intercomparison Project Phase 6 (CMIP6) experimental design and organization, *Geoscientific Model Development*,
1039 9, 1937–1958, <https://doi.org/10.5194/gmd-9-1937-2016>, 2016.

1040 Fischer, A. M., Strassmann, K. M., Croci-Maspoli, M., Hama, A. M., Knutti, R., Kotlarski, S., Schär, C., Schnadt Poberaj, C.,
1041 Ban, N., Bavay, M., Beyerle, U., Bresch, D. N., Brönnimann, S., Burlando, P., Casanueva, A., Fatichi, S., Feigenwinter, I.,
1042 Fischer, E. M., Hirschi, M., Liniger, M. A., Marty, C., Medhaug, I., Peleg, N., Pickl, M., Raible, C. C., Rajczak, J., Rössler,
1043 O., Scherrer, S. C., Schwierz, C., Seneviratne, S. I., Skelton, M., Sørland, S. L., Spirig, C., Tschurr, F., Zeder, J., and Zubler,
1044 E. M.: Climate Scenarios for Switzerland CH2018 – Approach and Implications, *Climate Services*, 26, 100288,
1045 <https://doi.org/10.1016/j.cliser.2022.100288>, 2022.

1046 François, B., Vrac, M., Cannon, A. J., Robin, Y., and Allard, D.: Multivariate bias corrections of climate simulations: which
1047 benefits for which losses?, *Earth System Dynamics*, 11, 537–562, <https://doi.org/10.5194/esd-11-537-2020>, 2020.

- 1048 Franke, J.: Rainfall complexity in mountains, *Nat. Clim. Chang.*, 14, 1223–1223, [https://doi.org/10.1038/s41558-024-02209-](https://doi.org/10.1038/s41558-024-02209-6)
1049 [6](https://doi.org/10.1038/s41558-024-02209-6), 2024.
- 1050 Frei, C., Christensen, J. H., De'que', M., Jacob, D., Jones, R. G., and Vidale, P. L.: Daily precipitation statistics in regional
1051 climate models: Evaluation and intercomparison for the European Alps. *J. Geophys. Res.*, 108, 4124,
1052 <https://doi.org/10.1029/2002JD002287>, 2003.
- 1053 Gaarder, J.E., Tajet, H.T.T., Dobler, A., Hygen, H.O. and Kvande, T.: Future Climate Projections and Uncertainty Evaluations
1054 for Frost Decay Exposure Index in Norway. *Buildings*, 14(9), p.2873, <https://doi.org/10.3390/buildings14092873>, 2024
- 1055 Golding, N., Lambkin, K., Wilson, L., Troch, R. D., Fischer, A. M., Hygen, H. O., Hama, A. M., Dyrddal, A. V., Jamsin, E.,
1056 Termonia, P., and Hewitt, C.: Developing national frameworks for climate services: Experiences, challenges and learnings
1057 from across Europe, *Climate Services*, 37, 100530, <https://doi.org/10.1016/j.cliser.2024.100530>, 2025.
- 1058 Gjertsen, A.K. and Nilsen, J.E.: SAT-SKOG: Et skogkart basert på tolking av satellittbilder. *Skog og landskap, rapport nr.*
1059 *23/2012*, 54 pp, <http://hdl.handle.net/11250/2453917> 2012.
- 1060 Gu, G. and Adler, R. F.: Spatial Patterns of Global Precipitation Change and Variability during 1901–2010,
1061 <https://doi.org/10.1175/JCLI-D-14-00201.1>, 2015.
- 1062 Gudmundsson, L.: qmap: Statistical Transformations for Post-Processing Climate Model Output, version 1.0-6,
1063 <https://doi.org/10.32614/CRAN.package.qmap>, 2025.
- 1064 Gudmundsson, L., Bremnes, J. B., Haugen, J. E., and Engen-Skaugen, T.: Technical Note: Downscaling RCM precipitation to
1065 the station scale using statistical transformations – a comparison of methods, *Hydrology and Earth System Sciences*,
1066 16, 3383–3390, <https://doi.org/10.5194/hess-16-3383-2012>, 2012.
- 1067 Gudmundsson, L., Boulange, J., Do, H. X., Gosling, S. N., Grillakis, M. G., Koutroulis, A. G., Leonard, M., Liu, J., Müller
1068 Schmied, H., Papadimitriou, L., Pokhrel, Y., Seneviratne, S. I., Satoh, Y., Thiery, W., Westra, S., Zhang, X., and Zhao, F.:
1069 Globally observed trends in mean and extreme river flow attributed to climate change, *Science*, 371, 1159–1162,
1070 <https://doi.org/10.1126/science.aba3996>, 2021.
- 1071 Gutiérrez, J. M., Maraun, D., Widmann, M., Huth, R., Hertig, E., Benestad, R., Roessler, O., Wibig, J., Wilcke, R., Kotlarski,
1072 S., San Martín, D., Herrera, S., Bedia, J., Casanueva, A., Manzanos, R., Iturbide, M., Vrac, M., Dubrovsky, M., Ribalaygua,
1073 J., Pórtoles, J., Rätty, O., Räisänen, J., Hingray, B., Raynaud, D., Casado, M. J., Ramos, P., Zerenner, T., Turco, M., Bosshard,
1074 T., Štěpánek, P., Bartholy, J., Pongracz, R., Keller, D. E., Fischer, A. M., Cardoso, R. M., Soares, P. M. M., Czernecki, B.,

1075 and Pagé, C.: An intercomparison of a large ensemble of statistical downscaling methods over Europe: Results from the
1076 VALUE perfect predictor cross-validation experiment, *International Journal of Climatology*, 39, 3750–3785,
1077 <https://doi.org/10.1002/joc.5462>, 2019.

1078 Hanssen-Bauer, I., Benestad, R.E., Lutz, J., Vikhamar-Schuler, D., Svyashchennikov, P. and Førland, E.J.: Comparative
1079 Analyses of Local Historical and Future Climate Conditions Important for Reindeer Herding in Finnmark, Norway and the
1080 Yamal Nenets Autonomous Okrug, Russia. In: Mathiesen, S.D., Eira, I.M.G., Turi, E.I., Oskal, A., Pogodaev, M., Tonkopeeva,
1081 M. (eds) *Reindeer Husbandry*. Springer Polar Sciences. Springer, Cham. https://doi.org/10.1007/978-3-031-17625-8_8, 2022

1082 Hanssen-Bauer, I., E.J. Førland, I. Haddeland, H. Hisdal, S. Mayer, A. Nesje, J.E. Ø. Nilsen, S. Sandven, A.B. Sandø, A. Sorteberg
1083 and B. Ådlandsvik: *Klima i Norge 2100 – Kunnskapsgrunnlag for klimatilpasning oppdatert i 2015*. Norsk Klimaservicesenter,
1084 NCCS Report 2/2015, 203pp, ISSN: 2387-3027, 2015.

1085 Hawkins, E. and Sutton, R.: The potential to narrow uncertainty in projections of regional precipitation change, *Clim Dyn*, 37,
1086 407–418, <https://doi.org/10.1007/s00382-010-0810-6>, 2011.

1087 Hersbach, H., Bell, B., Berrisford, P., Hirahara, S., Horányi, A., Muñoz-Sabater, J., Nicolas, J., Peubey, C., Radu, R., Schepers,
1088 D., Simmons, A., Soci, C., Abdalla, S., Abellan, X., Balsamo, G., Bechtold, P., Biavati, G., Bidlot, J., Bonavita, M., De Chiara,
1089 G., Dahlgren, P., Dee, D., Diamantakis, M., Dragani, R., Flemming, J., Forbes, R., Fuentes, M., Geer, A., Haimberger, L.,
1090 Healy, S., Hogan, R. J., Hólm, E., Janisková, M., Keeley, S., Laloyaux, P., Lopez, P., Lupu, C., Radnoti, G., de Rosnay, P.,
1091 Rozum, I., Vamborg, F., Villaume, S., and Thépaut, J.-N.: The ERA5 global reanalysis, *Quarterly Journal of the Royal*
1092 *Meteorological Society*, 146, 1999–2049, <https://doi.org/10.1002/qj.3803>, 2020.

1093 Hisdal, H., Vikhamar-Schuler, D., Førland, E., and Nilsen, I.: *Klimaprofiler for fylker*. (“Climate factsheets for counties”).
1094 NCCS Report 2/2021, Norwegian Centre for Climate Services, Oslo, Norway. (In Norwegian.).
1095 https://klimaservicesenter.no/kss/rapporter/rapporter-og-publikasjoner_2, 2021.

1096 Huang, S., Eisner, S., Magnusson, J. O., Lussana, C., Yang, X., and Beldring, S.: Improvements of the spatially distributed
1097 hydrological modelling using the HBV model at 1 km resolution for Norway, *Journal of Hydrology*, 577, 123585,
1098 <https://doi.org/10.1016/j.jhydrol.2019.03.051>, 2019.

1099 Huang, S., Eisner, S., Haddeland, I., and Tadege Mengistu, Z.: Evaluation of two new-generation global soil databases for
1100 macro-scale hydrological modelling in Norway, *Journal of Hydrology*, 610, 127895,
1101 <https://doi.org/10.1016/j.jhydrol.2022.127895>, 2022.

1102 Huang, S., Eisner, S., Wong, W. K., and Cattaneo, N.: The potential impacts of climate and forest changes on streamflow for
1103 micro-, meso- and macro-scale catchments in Norway, *Journal of Hydrology: Regional Studies*, 57, 102147,
1104 <https://doi.org/10.1016/j.ejrh.2024.102147>, 2025a.

1105 Huang, S., Haddeland, I., Lussana, C., Dobler, A., and Tveito, O.E.: Daily climate and hydrological reference data for Norway
1106 [Data set]. Dataset published 2025 via Norwegian Meteorological Institute, <https://doi.org/10.21343/gbq0-4t97>, 2025b.

1107 Huang, S., Wong, W.K., Tveito, O.E., Haddeland, I.: Impacts of empirical and physical evaporation methods on changes in
1108 hydrological components and drought indices under climate change scenarios, *Hydrology Research*, doi: 10.2166/nh.2026.220,
1109 2026.

1110 Hundecha, Y., Sunyer, M. A., Lawrence, D., Madsen, H., Willems, P., Bürger, G., Kriaučiūnienė, J., Loukas, A., Martinkova,
1111 M., Osuch, M., Vasiliades, L., von Christierson, B., Vormoor, K., and Yücel, I.: Inter-comparison of statistical downscaling
1112 methods for projection of extreme flow indices across Europe, *Journal of Hydrology*, 541, 1273–1286,
1113 <https://doi.org/10.1016/j.jhydrol.2016.08.033>, 2016.

1114 Huss, M., Jouviet, G., Farinotti, D., and Bauder, A.: Future high-mountain hydrology: a new parameterization of glacier retreat,
1115 *Hydrology and Earth System Sciences*, 14, 815–829, <https://doi.org/10.5194/hess-14-815-2010>, 2010.

1116 Hübener, H., Hoffmann, P., Keuler, K., Pfeifer, S., Ramthun, H., Spekat, A., Steger, C., and Warrach-Sagi, K.: Deriving user-
1117 informed climate information from climate model ensemble results, in: *Advances in Science and Research*, 16th EMS Annual
1118 Meeting & 11th European Conference on Applied Climatology (ECAC) -, 261–269, <https://doi.org/10.5194/asr-14-261-2017>,
1119 2017.

1120 IPCC: *Climate Change 2021: The Physical Science Basis*. Contribution of Working Group I to the Sixth Assessment Report
1121 of the Intergovernmental Panel on Climate Change [Masson-Delmotte, V., P. Zhai, A. Pirani, S.L. Connors, C. Péan, S. Berger,
1122 N. Caud, Y. Chen, L. Goldfarb, M.I. Gomis, M. Huang, K. Leitzell, E. Lonnoy, J.B.R. Matthews, T.K. Maycock, T. Waterfield,
1123 O. Yelekçi, R. Yu, and B. Zhou (eds.)]. Cambridge University Press, Cambridge, United Kingdom and New York, NY, USA,
1124 In press, doi:10.1017/9781009157896, 2021.

1125 Jacob, D., Petersen, J., Eggert, B., Alias, A., Christensen, O. B., Bouwer, L. M., Braun, A., Colette, A., Déqué, M., Georgievski,
1126 G., Georgopoulou, E., Gobiet, A., Menut, L., Nikulin, G., Haensler, A., Hempelmann, N., Jones, C., Keuler, K., Kovats, S.,
1127 Kröner, N., Kotlarski, S., Kriegsmann, A., Martin, E., van Meijgaard, E., Moseley, C., Pfeifer, S., Preuschmann, S.,
1128 Radermacher, C., Radtke, K., Rechid, D., Rounsevell, M., Samuelsson, P., Somot, S., Soussana, J.-F., Teichmann, C.,
1129 Valentini, R., Vautard, R., Weber, B., and Yiou, P.: EURO-CORDEX: new high-resolution climate change projections for
1130 European impact research, *Reg Environ Change*, 14, 563–578, <https://doi.org/10.1007/s10113-013-0499-2>, 2014.

- 1131 Jacob, D., Teichmann, C., Sobolowski, S., Katragkou, E., Anders, I., Belda, M., Benestad, R., Boberg, F., Buonomo, E.,
1132 Cardoso, R. M., Casanueva, A., Christensen, O. B., Christensen, J. H., Coppola, E., De Cruz, L., Davin, E. L., Dobler, A.,
1133 Domínguez, M., Fealy, R., Fernandez, J., Gaertner, M. A., García-Díez, M., Giorgi, F., Gobiet, A., Goergen, K., Gómez-
1134 Navarro, J. J., Alemán, J. J. G., Gutiérrez, C., Gutiérrez, J. M., Güttler, I., Haensler, A., Halenka, T., Jerez, S., Jiménez-
1135 Guerrero, P., Jones, R. G., Keuler, K., Kjellström, E., Knist, S., Kotlarski, S., Maraun, D., van Meijgaard, E., Mercogliano, P.,
1136 Montávez, J. P., Navarra, A., Nikulin, G., de Noblet-Ducoudré, N., Panitz, H.-J., Pfeifer, S., Piazza, M., Pichelli, E.,
1137 Pietikäinen, J.-P., Prein, A. F., Preuschmann, S., Rechid, D., Rockel, B., Romera, R., Sánchez, E., Sieck, K., Soares, P. M. M.,
1138 Somot, S., Srnec, L., Sørland, S. L., Termonia, P., Truhetz, H., Vautard, R., Warrach-Sagi, K., and Wulfmeyer, V.: Regional
1139 climate downscaling over Europe: perspectives from the EURO-CORDEX community, *Reg Environ Change*, 20, 51,
1140 <https://doi.org/10.1007/s10113-020-01606-9>, 2020.
- 1141 Katragkou, E., Sobolowski, S.P., Teichmann, C., Solmon, F., Pavlidis, V., Rechid, D., Hoffmann, P., Fernández, J., Nikulin,
1142 G. and Jacob, D.: Delivering an improved framework for the new generation of CMIP6-driven EURO-CORDEX regional
1143 climate simulations. *Bulletin of the American Meteorological Society*, 105(6), pp.E962-E974, [https://doi.org/10.1175/BAMS-](https://doi.org/10.1175/BAMS-D-23-0131.1)
1144 [D-23-0131.1](https://doi.org/10.1175/BAMS-D-23-0131.1), 2024.
- 1145 Kay, A. L.: A comparison of hydrological impacts from two ensembles of regional climate projections with a range of climate
1146 sensitivities, *Reg Environ Change*, 25, 89, <https://doi.org/10.1007/s10113-025-02426-5>, 2025.
- 1147 Kundzewicz, Z. W., Krysanova, V., Dankers, R., Hirabayashi, Y., Kanae, S., Hattermann, F. F., Huang, S., Milly, P. C. D.,
1148 Stoffel, M., Driessen, P. P. J., Matczak, P., Quevauviller, P., and Schellnhuber, H.-J.: Differences in flood hazard projections
1149 in Europe – their causes and consequences for decision making, *Hydrological Sciences Journal*, 62, 1–14,
1150 <https://doi.org/10.1080/02626667.2016.1241398>, 2017.
- 1151 Kuya, E. K., Hanssen-Bauer, I., Mayer, S., and Heiberg, H.: Projected changes of rain, sleet, and snowfall in Norway, *Norsk*
1152 *Geografisk Tidsskrift - Norwegian Journal of Geography*, 78, 73–87, <https://doi.org/10.1080/00291951.2024.2360409>, 2024.
- 1153 Lafferty, D. C. and Sriver, R. L.: Downscaling and bias-correction contribute considerable uncertainty to local climate
1154 projections in CMIP6, *npj Clim Atmos Sci*, 6, 158, <https://doi.org/10.1038/s41612-023-00486-0>, 2023.
- 1155 Lawrence, D.: Uncertainty introduced by flood frequency analysis in projections for changes in flood magnitudes under a
1156 future climate in Norway. *Journal of Hydrology: Regional Studies* 28:100675, <https://doi.org/10.1016/j.ejrh.2020.100675>,
1157 2020.

- 1158 Li, H., Beldring, S., Xu, C.-Y., Huss, M., Melvold, K., and Jain, S. K.: Integrating a glacier retreat model into a hydrological
1159 model – Case studies of three glacierised catchments in Norway and Himalayan region, *Journal of Hydrology*, 527, 656–667,
1160 <https://doi.org/10.1016/j.jhydrol.2015.05.017>, 2015.
- 1161 Li, L., Wang, B., Feng, P., Jägermeyr, J., Asseng, S., Müller, C., Macadam, I., Liu, D. L., Waters, C., Zhang, Y., He, Q., Shi,
1162 Y., Chen, S., Guo, X., Li, Y., He, J., Feng, H., Yang, G., Tian, H., and Yu, Q.: The optimization of model ensemble composition
1163 and size can enhance the robustness of crop yield projections, *Commun Earth Environ*, 4, 362, [https://doi.org/10.1038/s43247-](https://doi.org/10.1038/s43247-023-01016-9)
1164 [023-01016-9](https://doi.org/10.1038/s43247-023-01016-9), 2023.
- 1165 Liersch, S., Drews, M., Pilz, T., Salack, S., Sietz, D., Aich, V., A D Larsen, M., Gädeke, A., Halsnæs, K., Thiery, W., Huang,
1166 S., Lobanova, A., Koch, H., and Hattermann, F. F.: One simulation, different conclusions—the baseline period makes the
1167 difference!, *Environ. Res. Lett.*, 15, 104014, <https://doi.org/10.1088/1748-9326/aba3d7>, 2020.
- 1168 Lussana, C: seNorge observational gridded datasets, MET report 7-2020, [https://www.met.no/publikasjoner/met-report/met-](https://www.met.no/publikasjoner/met-report/met-report-2020/_attachment/download/9f79d391-62d8-4fc1-a61a-9f0e7f1de389:8c74ebf2118593aa75272e6aff416ce66f86e73f/MET-report-07-2020.pdf)
1169 [report-2020/_attachment/download/9f79d391-62d8-4fc1-a61a-](https://www.met.no/publikasjoner/met-report/_attachment/download/9f79d391-62d8-4fc1-a61a-9f0e7f1de389:8c74ebf2118593aa75272e6aff416ce66f86e73f/MET-report-07-2020.pdf)
1170 [9f0e7f1de389:8c74ebf2118593aa75272e6aff416ce66f86e73f/MET-report-07-2020.pdf](https://www.met.no/publikasjoner/met-report/_attachment/download/9f79d391-62d8-4fc1-a61a-9f0e7f1de389:8c74ebf2118593aa75272e6aff416ce66f86e73f/MET-report-07-2020.pdf), 2020.
- 1171 Lussana, C., Tveito, O. E., Dobler, A., and Tunheim, K.: seNorge_2018, daily precipitation, and temperature datasets over
1172 Norway, *Earth System Science Data*, 11, 1531–1551, <https://doi.org/10.5194/essd-11-1531-2019>, 2019.
- 1173 Lutz, J., Hanssen-Bauer, I., Tveito, O. E. and Dobler, A.: Precipitation variability in Norway 1961–2020. MET-report 01-
1174 2024, [https://www.met.no/publikasjoner/met-report/_attachment/download/f5ba4d69-dba2-4eb6-bed9-](https://www.met.no/publikasjoner/met-report/_attachment/download/f5ba4d69-dba2-4eb6-bed9-0189178b5e7a:ba4f4974e503f9509d33f101efc40145b47a59e6/MET%20report%201%202024.pdf)
1175 [0189178b5e7a:ba4f4974e503f9509d33f101efc40145b47a59e6/MET%20report%201%202024.pdf](https://www.met.no/publikasjoner/met-report/_attachment/download/f5ba4d69-dba2-4eb6-bed9-0189178b5e7a:ba4f4974e503f9509d33f101efc40145b47a59e6/MET%20report%201%202024.pdf), 2024.
- 1176 Majasalmi, T., Eisner, S., Astrup, R., Fridman, J., and Bright, R. M.: An enhanced forest classification scheme for modeling
1177 vegetation–climate interactions based on national forest inventory data, *Biogeosciences*, 15, 399–412,
1178 <https://doi.org/10.5194/bg-15-399-2018>, 2018.
- 1179 Maraun, D.: Bias Correction, Quantile Mapping, and Downscaling: Revisiting the Inflation Issue. *Journal of Climate*, 26,
1180 2137–2143, <https://doi.org/10.1175/jcli-d-12-00821.1>, 2013.
- 1181 Maraun, D. and Widmann, M.: *Statistical Downscaling and Bias Correction for Climate Research*. Cambridge University
1182 Press, 347 pp, 2018.
- 1183 Martinich, J. and Crimmins, A.: Climate damages and adaptation potential across diverse sectors of the United States, *Nature*
1184 *Climate Change*, 9, 397-404, 2019.
- 1185 Matiu, M., Napoli, A., Kotlarski, S., Zardi, D., Bellin, A., and Majone, B.: Elevation-dependent biases of raw and bias-
1186 adjusted EURO-CORDEX regional climate models in the European Alps, *Climate Dynamics*,
1187 <https://doi.org/10.1007/s00382-024-07376-y>, 2024.

- 1188 Mayer, S., Khasandi Kuya, E., Antonsen, K., Abegg, B., and Hanssen-Bauer, I.: Warmer and wetter: Outlining climate services
1189 for snow-dependent tourism in Norway – The case of Lofoten, *Climate Services*, 32, 100405,
1190 <https://doi.org/10.1016/j.cliser.2023.100405>, 2023.
- 1191 McAfee, S. A.: Methodological differences in projected potential evapotranspiration, *Climatic Change*, 120, 915–930,
1192 <https://doi.org/10.1007/s10584-013-0864-7>, 2013.
- 1193 McSweeney, C. F., Jones, R. G., Lee, R. W., and Rowell, D. P.: Selecting CMIP5 GCMs for downscaling over multiple
1194 regions, *Clim Dyn*, 44, 3237–3260, <https://doi.org/10.1007/s00382-014-2418-8>, 2015.
- 1195 Mehrotra, R. and Sharma, A.: A Resampling Approach for Correcting Systematic Spatiotemporal Biases for Multiple Variables
1196 in a Changing Climate, *Water Resources Research*, 55, 754–770, <https://doi.org/10.1029/2018WR023270>, 2019.
- 1197 Meyer, J., Kohn, I., Stahl, K., Hakala, K., Seibert, J., and Cannon, A. J.: Effects of univariate and multivariate bias correction
1198 on hydrological impact projections in alpine catchments, *Hydrol. Earth Syst. Sci.*, 23, 1339–1354, [https://doi.org/10.5194/hess-](https://doi.org/10.5194/hess-23-1339-2019)
1199 [23-1339-2019](https://doi.org/10.5194/hess-23-1339-2019), 2019.
- 1200 Moriasi, D. N., Arnold, J. G., Liew, M. W. V., Bingner, R. L., Harmel, R. D., and Veith, T. L.: Model Evaluation Guidelines
1201 for Systematic Quantification of Accuracy in Watershed Simulations, *Transactions of the ASABE*, 50, 885–900,
1202 <https://doi.org/10.13031/2013.23153>, 2007.
- 1203 Müller, M., Homleid, M., Ivarsson, K.-I., Køltzow, M. A. Ø., Lindskog, M., Midtbø, K. H., Andrae, U., Aspelien, T., Berggren,
1204 L., Bjørge, D., Dahlgren, P., Kristiansen, J., Randriamampianina, R., Ridal, M., and Vignes, O.: AROME-MetCoOp: A Nordic
1205 Convective-Scale Operational Weather Prediction Model, <https://doi.org/10.1175/WAF-D-16-0099.1>, 2017.
- 1206 Nash, J.E. and Sutcliffe, J.V.: River flow forecasting through conceptual models part I -A discussion of principles, *J Hydrol*,
1207 10, 282–290, 1970.
- 1208 Nilsen, I. B., Hanssen-Bauer, I., Tveito, O. E., and Wong, W. K.: Projected changes in days with zero-crossings for Norway,
1209 *International Journal of Climatology*, 41, 2173–2188, <https://doi.org/10.1002/joc.6913>, 2021.
- 1210 Nilsen, I. B., Hanssen-Bauer, I., Dyrødal, A. V., Hisdal, H., Lawrence, D., Haddeland, I., and Wong, W. K.: From Climate
1211 Model Output to Actionable Climate Information in Norway, *Front. Clim.*, 4, <https://doi.org/10.3389/fclim.2022.866563>,
1212 2022.
- 1213 Norwegian Government: Statlige Planretningslinjer for klima- og energi. (“government guidelines on climate and renergy”),
1214 available online at: <https://lovdata.no/dokument/SF/forskrift/2024-12-20-3359> (accessed December 06. October 2025), 2024.

- 1215 Padrón, R. S., Gudmundsson, L., Decharme, B., Ducharne, A., Lawrence, D. M., Mao, J., Peano, D., Krinner, G., Kim, H.,
1216 and Seneviratne, S. I.: Observed changes in dry-season water availability attributed to human-induced climate change, *Nat.*
1217 *Geosci.*, 13, 477–481, <https://doi.org/10.1038/s41561-020-0594-1>, 2020.
- 1218 Paz, S.M. and Willems, P.: Uncovering the strengths and weaknesses of an ensemble of quantile mapping methods for
1219 downscaling precipitation change in Southern Africa. *J. Hydrol. -Reg. Stud.* 41, 101104,
1220 <https://doi.org/10.1016/j.ejrh.2022.101104>, 2022.
- 1221 Peter, J., Vogel, E., Sharples, W., Bende-Michl, U., Wilson, L., Hope, P., Dowdy, A., Kociuba, G., Srikanthan, S., Duong, V.
1222 C., Roussis, J., Matic, V., Khan, Z., Oke, A., Turner, M., Baron-Hay, S., Johnson, F., Mehrotra, R., Sharma, A., Thatcher, M.,
1223 Azarvinand, A., Thomas, S., Boschat, G., Donnelly, C., and Argent, R.: Continental-scale bias-corrected climate and
1224 hydrological projections for Australia, *Geoscientific Model Development*, 17, 2755–2781, [https://doi.org/10.5194/gmd-17-](https://doi.org/10.5194/gmd-17-2755-2024)
1225 [2755-2024](https://doi.org/10.5194/gmd-17-2755-2024), 2024.
- 1226 Pirk, N., Aalstad, K., Yilmaz, Y. A., Vatne, A., Popp, A. L., Horvath, P., Bryn, A., Vollsnes, A. V., Westermann, S., Berntsen,
1227 T. K., Stordal, F., and Tallaksen, L. M.: Snow–vegetation–atmosphere interactions in alpine tundra, *Biogeosciences*, 20, 2031–
1228 2047, <https://doi.org/10.5194/bg-20-2031-2023>, 2023.
- 1229 Pourmokhtarian, A., Driscoll, C. T., Campbell, J. L., Hayhoe, K., and Stoner, A. M. K.: The effects of climate downscaling
1230 technique and observational data set on modeled ecological responses, *Ecological Applications*, 26, 1321–1337,
1231 <https://doi.org/10.1890/15-0745>, 2016.
- 1232 Reistad, M., Øyvind Breivik, Haakenstad, H., Aarnes, O. J., Furevik, B. R., and Bidlot, J.-R.: A high-resolution hindcast of
1233 wind and waves for the North Sea, the Norwegian Sea, and the Barents Sea, *J. Geophys. Res.*, 116,
1234 <https://doi.org/10.1029/2010JC006402>, 2011.
- 1235 Reyniers, N., Zha, Q., Addor, N., Osborn, T. J., Forstenhäusler, N., and He, Y.: Two sets of bias-corrected regional UK Climate
1236 Projections 2018 (UKCP18) of temperature, precipitation and potential evapotranspiration for Great Britain, *Earth System*
1237 *Science Data*, 17, 2113–2133, <https://doi.org/10.5194/essd-17-2113-2025>, 2025.
- 1238 Rössler, O., Fischer, A. M., Huebener, H., Maraun, D., Benestad, R. E., Christodoulides, P., Soares, P. M. M., Cardoso, R. M.,
1239 Pagé, C., Kanamaru, H., Kreienkamp, F., and Vlachogiannis, D.: Challenges to link climate change data provision and user
1240 needs: Perspective from the COST-action VALUE, *International Journal of Climatology*, 39, 3704–3716,
1241 <https://doi.org/10.1002/joc.5060>, 2019.
- 1242 Statistics Norway: [Land use and land cover – SSB](#), last accessed on 27.03.2025, 2025.

- 1243 Schumacher, D.L., Singh, J., Hauser, M., Fischer, E.M., Wild, M. and Seneviratne, S.I.: Exacerbated summer European
1244 warming not captured by climate models neglecting long-term aerosol changes. *Communications Earth & Environment*, 5(1),
1245 p.182, <https://doi.org/10.1038/s43247-024-01332-8>, 2024.
- 1246 Sobolowski, S., Somot, S., Fernandez, J., Evin, G., Brands, S., Maraun, D., Kotlarski, S., Jury, M., Benestad, R.E., Teichmann,
1247 C. and Christensen, O.B.: GCM Selection and Ensemble Design: Best Practices and Recommendations from the EURO-
1248 CORDEX Community, *Bulletin of the American Meteorological Society*, 106(9), pp.E1834-E1850,
1249 <https://doi.org/10.1175/BAMS-D-23-0189.1>, 2025.
- 1250 Tam, B., Bonsal, B., Zhang, X., Zhang, Q., and Rong, R.: Assessing Potential Evapotranspiration Methods in Future Drought
1251 Projections across Canada, *Atmosphere-Ocean*, 62, 193–205, <https://doi.org/10.1080/07055900.2023.2288632>, 2024.
- 1252 Tang, J., Niu, X., Wang, S., Gao, H., Wang, X., and Wu, J.: Statistical downscaling and dynamical downscaling of regional
1253 climate in China: Present climate evaluations and future climate projections, *Journal of Geophysical Research: Atmospheres*,
1254 121, 2110–2129, <https://doi.org/10.1002/2015JD023977>, 2016.
- 1255 Taylor, K. E., Stouffer, R. J., and Meehl, G. A.: An overview of CMIP5 and the experiment design, *B. Am. Meteorol. Soc.*,
1256 93, 485–498, <https://doi.org/10.1175/BAMS-D-11-00094.1>, 2012.
- 1257 Thorarinsdottir, T. L., Gneiting, T., and Gissibl, N.: Using proper divergence functions to evaluate climate models. *SIAM-*
1258 *ASA J. Uncertainty Quantif.*, 1, 522–534, <https://doi.org/10.1137/130907550>, 2013.
- 1259 Tong, Y., Gao, X., Han, Z., Xu, Y. and Giorgi, F.: Bias correction of temperature and precipitation over China for RCM
1260 simulations using the QM and QDM methods, *Climate Dynamics* 57, 1425-1443, [https://doi.org/10.1007/s00382-020-05447-](https://doi.org/10.1007/s00382-020-05447-4)
1261 [4](https://doi.org/10.1007/s00382-020-05447-4), 2021.
- 1262 Tveito, O. E.: Norwegian standard climate normals 1991-2020 – the methodological approach, MET report 5 2021,
1263 [https://www.met.no/publikasjoner/met-report/met-report-2021/_/attachment/download/31bb0160-d8cf-4a2b-9646-](https://www.met.no/publikasjoner/met-report/met-report-2021/_/attachment/download/31bb0160-d8cf-4a2b-9646-4df6f5904059:3ac4fec6cf3fb7919ae42db2b63ad8e8b9e6a6/METreport%2005_2021_New_Norwegian_standard_climate_normals_1991_2020-signert.pdf)
1264 [4df6f5904059:3ac4fec6cf3fb7919ae42db2b63ad8e8b9e6a6/METreport%2005_2021_New_Norwegian_standard_climate_](https://www.met.no/publikasjoner/met-report/met-report-2021/_/attachment/download/31bb0160-d8cf-4a2b-9646-4df6f5904059:3ac4fec6cf3fb7919ae42db2b63ad8e8b9e6a6/METreport%2005_2021_New_Norwegian_standard_climate_normals_1991_2020-signert.pdf)
1265 [normals_1991_2020-signert.pdf](https://www.met.no/publikasjoner/met-report/met-report-2021/_/attachment/download/31bb0160-d8cf-4a2b-9646-4df6f5904059:3ac4fec6cf3fb7919ae42db2b63ad8e8b9e6a6/METreport%2005_2021_New_Norwegian_standard_climate_normals_1991_2020-signert.pdf), 2021.
- 1266 Vautard, R., Kadyrov, N., Iles, C., Boberg, F., Buonomo, E., Bülow, K., Coppola, E., Corre, L., van Meijgaard, E.,
1267 Nogherotto, R., Sandstad, M., Schwingshackl, C., Somot, S., Aalbers, E., Christensen, O. B., Ciarlo, J. M., Demory, M.-E.,
1268 Giorgi, F., Jacob, D., Jones, R. G., Keuler, K., Kjellström, E., Lenderink, G., Levvasseur, G., Nikulin, G., Sillmann, J.,
1269 Solidoro, C., Sørland, S. L., Steger, C., Teichmann, C., Warrach-Sagi, K., and Wulfmeyer, V.: Evaluation of the Large EURO-

1270 CORDEX Regional Climate Model Ensemble, *Journal of Geophysical Research: Atmospheres*, 126, e2019JD032344,
1271 <https://doi.org/10.1029/2019JD032344>, 2021.

1272 Vetter, T., Reinhardt, J., Flörke, M., van Griensven, A., Hattermann, F., Huang, S., Koch, H., Pechlivanidis, I. G., Plötner, S.,
1273 Seidou, O., Su, B., Vervoort, R. W., and Krysanova, V.: Evaluation of sources of uncertainty in projected hydrological changes
1274 under climate change in 12 large-scale river basins, *Climatic Change*, 141, 419–433, <https://doi.org/10.1007/s10584-016-1794->
1275 [y](https://doi.org/10.1007/s10584-016-1794-y), 2017.

1276 Wang, X. and Liu, L.: The Impacts of Climate Change on the Hydrological Cycle and Water Resource Management, *Water*,
1277 15, 2342, <https://doi.org/10.3390/w15132342>, 2023.

1278 Wilkinson, M. D., Dumontier, M., Aalbersberg, Ij. J., Appleton, G., Axton, M., Baak, A., Blomberg, N., Boiten, J.-W., da
1279 Silva Santos, L. B., Bourne, P. E., Bouwman, J., Brookes, A. J., Clark, T., Crosas, M., Dillo, I., Dumon, O., Edmunds, S.,
1280 Evelo, C. T., Finkers, R., Gonzalez-Beltran, A., Gray, A. J. G., Groth, P., Goble, C., Grethe, J. S., Heringa, J., 't Hoen, P. A.
1281 C., Hooft, R., Kuhn, T., Kok, R., Kok, J., Lusher, S. J., Martone, M. E., Mons, A., Packer, A. L., Persson, B., Rocca-Serra, P.,
1282 Roos, M., van Schaik, R., Sansone, S.-A., Schultes, E., Sengstag, T., Slater, T., Strawn, G., Swertz, M. A., Thompson, M., van
1283 der Lei, J., van Mulligen, E., Velterop, J., Waagmeester, A., Wittenburg, P., Wolstencroft, K., Zhao, J., and Mons, B.: The
1284 FAIR Guiding Principles for scientific data management and stewardship, *Sci Data*, 3, 160018,
1285 <https://doi.org/10.1038/sdata.2016.18>, 2016.

1286 Wolff, M. A., Isaksen, K., Petersen-Øverleir, A., Ødemark, K., Reitan, T., and Brækkan, R.: Derivation of a new continuous
1287 adjustment function for correcting wind-induced loss of solid precipitation: results of a Norwegian field study, *Hydrology and*
1288 *Earth System Sciences*, 19, 951–967, <https://doi.org/10.5194/hess-19-951-2015>, 2015.

1289 Wong, W.K., Dobler, A., Huang, S., Beldring, S., Melvold, K., Ruan, G.: Daily bias-adjusted climate (COR-BA-2025) and
1290 hydrological (distHBV-COR-BA-2025) projections for Norway [Data set]. Dataset published 2025 via Norwegian
1291 Meteorological Institute <https://doi.org/10.21343/0k90-6w67>, 2025

1292 Wong, W.K., Haddeland, I., Lawrence, D., and Beldring, S.: Gridded 1x1 km climate and hydrological projections for Norway.
1293 NVE Report No. 59, Norwegian Water Resources and Energy Directorate, Oslo, Norway, 2016.

1294 Yilmaz, K. K., Gupta, H. V., and Wagener, T.: A process-based diagnostic approach to model evaluation: Application to the
1295 NWS distributed hydrologic model, *Water Resources Research*, 44, <https://doi.org/10.1029/2007WR006716>, 2008.

- 1296 Yuan, Q., Thorarinsdottir, T. L., Beldring, S., Wong, W. K., Huang, S., and Xu, C.-Y.: New Approach for Bias Correction and
1297 Stochastic Downscaling of Future Projections for Daily Mean Temperatures to a High-Resolution Grid, *J. Appl. Meteorol.*
1298 *Clim.*, 58, 2617–2632, <https://doi.org/10.1175/JAMC-D-19-0086.1>, 2019.
- 1299 Yuan Q., Thorarinsdottir T.L., Beldring S., Wong W.K., and Xu C.-Y.: Bridging the scale gap: obtaining high-resolution
1300 stochastic simulations of gridded daily precipitation in a future climate, *Hydrol. Earth Syst. Sci.*, 25 (9), pp. 5259-5275,
1301 <https://doi.org/10.5194/hess-25-5259-2021>, 2021.
- 1302 Zhang, H., Chapman, S., Trancoso, R., Toombs, N. and Syktus, J.: Assessing the impact of bias correction approaches on
1303 climate extremes and the climate change signal, *Meteorol. Appl.*, 31, 1-18, <https://doi.org/10.1002/met.2204>, 2024.
- 1304 Zhang, L., Xu, Y., Meng, C., Li, X., Liu, H., and Wang, C.: Comparison of Statistical and Dynamic Downscaling Techniques
1305 in Generating High-Resolution Temperatures in China from CMIP5 GCMs, <https://doi.org/10.1175/JAMC-D-19-0048.1>,
1306 2020.
- 1307